Lithos 134-135 (2012) 163–178

Contents lists available at SciVerse ScienceDirect

Lithos

journal homepage: www.elsevier.com/locate/lithos

The Cretaceous adakitic–basaltic–granitic magma sequence on south-eastern margin of the North China Craton: Implications for lithospheric thinning mechanism

Sheng-Ao Liu [a,*], Shuguang Li [a,b,*], Sushu Guo [a], Zhenhui Hou [a], Yongsheng He [b]

[a] CAS Key Laboratory of Crust-Mantle Materials and Environments, School of Earth and Space Sciences, University of Science and Technology of China, Hefei 230026, China
[b] State Key Laboratory of Geological Processes and Mineral Resources, China University of Geosciences, Beijing 100083, China

ARTICLE INFO

Article history:
Received 24 August 2011
Accepted 29 December 2011
Available online 8 January 2012

Keywords:
Adakite
Granitoid
Diabase
Foundering
Lithospheric thinning
North China Craton

ABSTRACT

We present here a combined study of Early Cretaceous granodiorites, granites and mafic rocks from the Bengbu area on south-eastern margin of the North China Craton (NCC), in order to provide insights into the thinning mechanism of lithosphere on the cratonic margins. Zircon U–Pb and Ar–Ar dating reveals an adakitic–basaltic–granitic magma sequence with the adakitic intrusions (granodiorites; 123–115 Ma) formed prior to the granites and mafic dykes (both ca.112 Ma). The granodiorites are geochemically similar to low-Mg# adakitic rocks and isotopically have enriched Sr–Nd–Hf compositions, low radiogenic Pb ($^{206}Pb/^{204}Pb_i = 16.524–17.017$), and mantle-like $\delta^{18}O_{zircon}$ ($5.8 \pm 0.5‰$). They were originated from the thickened lower continental crust (LCC) of the NCC. In contrast, the granites have low Sr/Y (<20), La/Yb_N, Dy/Yb_N, and prominent negative Eu anomalies, indicating their origination at the shallow middle-lower crustal levels. The mafic dykes are enriched in LREE relative to HREE, and exhibit negative anomalies of Nb, Ta, Ti and positive anomalies of Pb. They have low Nb/U, Ce/Pb, high La/Nb, Ba/Nb, enriched Sr–Nd isotopic compositions and low radiogenic Pb ($^{206}Pb/^{204}Pb_i = 16.789$ to 17.262), indicating LCC materials involved into the mantle sources. Modeling suggests derivation of the mafic dykes from the depleted upper mantle hybridized by 10–15% recycled LCC. The contrasting chemical characteristics of adakitic rocks and granites imply that recycling of the LCC was likely achieved through rapid foundering at 115–112 Ma, which resulted in thinning of the overlying crust and hybridization of the underlying mantle with closely coeval generation of granitic and basaltic magmas. Anatexis of the pre-existing thickened LCC at 123–115 Ma that attenuated the LCC itself and left the residues denser as a result of felsic (adakitic) melt extraction is proposed to have resulted in gravitational instability and foundering of the lithosphere. Such a temporal sequence of magma generation and processes of lithospheric thinning also occurred on north margin of the NCC and are quite similar to the mountain-root removal beneath the Dabie Orogen in central China. This manifests that previous melting of the LCC is perhaps an important trigger responsible for lithospheric foundering in orogenic belts and cartonic margins, where the lithosphere underwent pre-thickening by continental collisions and had stabilized over a long time.

1. Introduction

The lithospheric keel of an Archean craton could have kept gravitationally stable over the geologic history due to its inherent neutral or positive buoyancy and highly melt-depleted characteristic. However, the North China Craton (NCC) has been taken as a classic example that the Archean thick/cold lithospheric keel in the eastern NCC appears to have been partially, or even wholly removed and replaced with a newly accreted, hot lithosphere (Fan and Menzies, 1992; Fan et al., 2000; Griffin et al., 1998; Menzies et al., 1993). In the past two decades, lots of studies covering aspects of geology, geochemistry and geophysics have attempted to place constraints on timing and mechanism of the lithospheric thinning (Menzies et al., 2007 and reference therein). To date, although there is general consensus on the timing of lithospheric thinning (i.e. during the Mesozoic), the questions concerning the mechanisms and processes are still open.

The temporal duration and formation sequence of various types of magmatism are pivotal to understanding the mechanism and processes of lithospheric thinning during the Mesozoic. For example, the long term (~100 Ma) activity of Mesozoic magmatism throughout the entire NCC has been considered as the key evidence for the protracted thermo-chemical erosion model (Menzies et al., 2007; Xu et al., 2004). Mesozoic magmatism throughout the NCC, however, had a peak within a short duration (125 ± 5 Ma) during the Early Cretaceous (Wu et al., 2005a), and in many regions it was discrete comprising multiple episodes (e.g., Yang et al., 2008). Alternatively, an "opposite" model emphasizing rapid delamination or foundering of the over-thickened lower continental crust (LCC) together with the

* Correspondence to: S.-A. Liu, School of the Earth Science and Resources, China University of Geosciences, Beijing 100083, China. Tel./fax: +86 551 3607647.
E-mail addresses: lsa@mail.ustc.edu.cn (S.-A. Liu), lsg@ustc.edu.cn (S. Li).

0024-4937/$ – see front matter © 2012 Elsevier B.V. All rights reserved.
doi:10.1016/j.lithos.2011.12.015

underlying lithospheric mantle, was proposed by many scientists as a possible mechanism responsible for the Mesozoic lithospheric thinning and the huge amounts of Early Cretaceous magmatism in the NCC (Gao et al., 2004; Ling et al., 2009; Liu et al., 2008, 2009a; Xu et al., 2006b; Yang et al., 2005). Delamination seems to be successful in explaining the genesis of some high-Mg# adakitic rocks and recycling lower crustal components observed in mantle source regions of Mesozoic basaltic rocks, as reported by these above studies. However, the trigger mechanism for lithospheric delamination has been frequently questioned and remains not well constrained, since the lower crustal eclogite layer taking along the buoyant mantle lithosphere may be insufficient to create enough gravitational instability and induce delamination.

Recent studies on post-collisional igneous rocks from the Dabie Orogen (central China) suggest that partial melting of the thickened lower crust may trigger foundering of the mountain keel (He et al., 2011), followed by partial melting of upwelling mantle and shallow crust in a short timescale (e.g. ≤10 Ma), typically generating an adakitic–basaltic–granitic magma sequence (He et al., 2011; Wang et al., 2007). Therefore, it is interesting to investigate whether similar sequences of magma formation also occur in the NCC, which would have broad significance for understanding the mechanism of lithospheric thinning in the on-craton regions.

In this paper, we report combined chronological and geochemical studies for Early Cretaceous granitoids and mafic rocks from the Bengbu area on the south-eastern margin of the NCC. Our results show that Early Cretaceous igneous rocks in the Bengbu area were formed within a short timescale (~10 Ma) with adakitic rocks prior to mafic rocks and normal granites, similar to the case of the Dabie Orogen, and the mafic rocks show evidence for involvement of the recycled lower crust. We proposed a two-stage model of lithospheric thinning to explain these observations with the emphasis of the key role of previous partial melting of thickened lower crust and extraction of felsic melts in creating gravitational instability of the lithosphere.

2. Geological setting and sample petrology

2.1. Geology of the Bengbu uplift

Eastern China comprises two major tectonic units: the NCC and the South China block (SCB) (Fig. 1a). They are separated by the Triassic Dabie–Sulu orogen that was formed during continent–continent collision between these two blocks (Li et al., 1993, 2000). The basement of the NCC consists primarily of Early to Late Archean high- and low-grade TTG gneisses and syntectonic granitoids, and supracrustal rocks as well as some Early Proterozoic magma-tectonic belts (Zhao et al., 2001). The Bengbu area, located ~150 km north of the Dabie Orogen, is an uplift region on the south-eastern margin of the NCC, bounded by the Tan–Lu Fault on the east and the Hefei basin on the south (Fig. 1a).

Exposed basement rocks in Bengbu area mainly include the Archean Complex of the Wuhe Group, together with appearance of several Early Proterozoic intrusions. Previous geochronological studies of

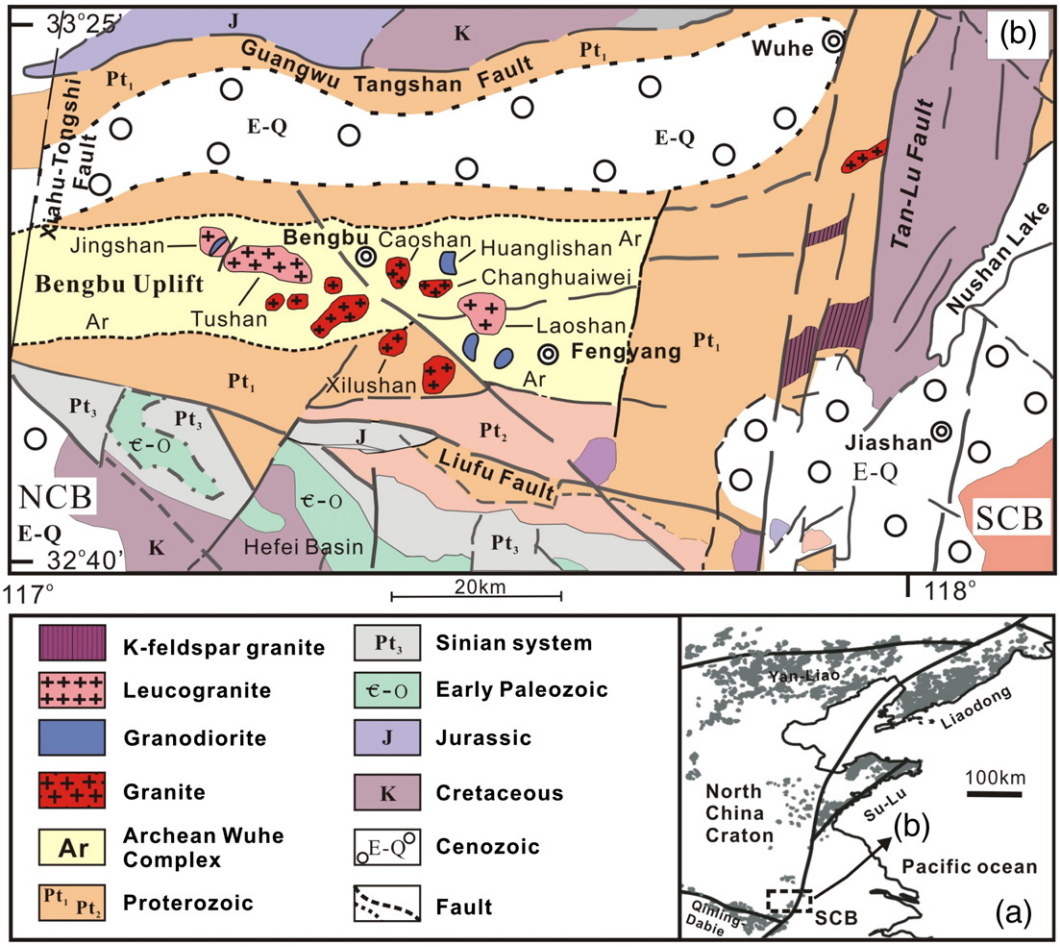

Fig. 1. (a) Spatial distribution of Mesozoic igneous rocks in the eastern North China Craton (modified from Yang et al., 2008). SCB represents the South China Block. (b) Detailed geological map showing regional locations of Mesozoic granitoids in the Bengbu area. Mafic dyke swarms intruded into leucogranites in Jingshan and into granodiorites in Huanglishan. The outcrops (~2–5 m width) of the mafic dykes are too small to plot in this map.

zircons and petrological studies of mineral inclusions in zircons show that the Wuhe Complex was subjected to large-scale high-grade (up to high-pressure granulite-facies) metamorphism in the Paleoproterozoic and tectonically belongs to part of the NCC basement (Guo and Li, 2009b; Liu et al., 2009b). The high-pressure granulite-facies metamorphic complex underwent widespread amphibolite-facies regression overprinting probably in the Mesozoic (Liu et al., 2009b). Voluminous Mesozoic granitoids (Fig. 1b) intruded into the Wuhe Complex in the Late Jurassic (~160 Ma) and in the Early to middle-Early Cretaceous (130–112 Ma). The Late Jurassic granitoids consist predominantly of garnet-bearing leucogranite (Guo and Li, 2009a) and the Cretaceous granitoids include a wide range of lithology of syenogranite, granodiorite and monzogranite (Yang et al., 2010). A small amount of mafic igneous rocks (mainly diabase dykes) are also exposed in the Bengbu area, which have not been investigated previously but comprise the focus of the present study.

Recent studies identified Neoproterozoic igneous zircons and Triassic metamorphic zircons in the Bengbu Jurassic leucogranites (Xu et al., 2005a; Yang et al., 2010), which are similar to those observed in the Dabie–Sulu ultra-high pressure metamorphic rocks, suggesting that the crustal materials of the SCB had been subducted or injected to the Bengbu area. This, along with the occurrence of eclogite xenoliths in ~130 Ma high-Mg# diorites from the Xu-Huai area located ~100 km north of the Bengbu (Xu et al., 2006a), imply that the crust on south-eastern margin of the NCC may have been thickened by injection or other mechanisms since the Early Cretaceous, at least. Therefore, Bengbu provides an ideal case to study the mechanism and processes of thinning of the pre-existing thickened LCC and the underlying lithospheric mantle in the NCC.

2.2. Samples

Total 26 samples were collected for this study, including 15 from two granodiorite plutons (Huanglishan and Jingshan), 9 from two mafic dykes (Huanglishan and Jingshan), and 2 from one granite pluton (Changhuaiwei). The Jingshan granodiorites (e.g., sample JS-5) or porphyry granodiorites (sample 04JS-3) (coordinates: N32°57′06″, E117°11′5.3″) occur as small bodies intruded into the Late Jurassic leucogranite. The granodiorites show a coarse granular texture and are composed of plagioclase (40–45%), alkali feldspar (25–30%), quartz (20–25%), hornblende (1–2%), and biotite (5–10%), as well as accessory magnetite, zircon and apatite. In the Jingshan area, diabase dyke swarms (~2–5 m width) cut through the Jurassic leucogranite, but their contact relationship with the granodiorite pluton is not clearly visible. The diabases have a visible texture of euhedral lath-shaped plagioclase crystals with the matrix generally having clinopyroxene, magnetite and phlogopite.

The Huanglishan granodiorite pluton (coordinates: N32°56′4.4″, E117°27′15.2″) is located ~40 km east of the Jingshan pluton. It intruded into the Wuhe metamorphic Complex, with an exposure outcrop of ~4 km^2. These granodiorites have a mineral assemblage of plagioclase (40–45%), quartz (25–30%), alkali feldspar (15–25%), hornblende (2–5%), biotite (5–10%), and accessory magnetite, zircon and apatite. In the Huanglishan area, diabase dyke swarms (~2 m width) cut through the granodiorite pluton in which the intrusive contact relationships are clearly observed, and thus, the diabase dykes must have formed subsequent to the granodiorite pluton. The texture and mineralogy of the Huanglishan diabase dykes are similar to those of the Jingshan diabase dykes.

The Changhuaiwei pluton is mainly composed of monzogranite. It is located ~1 km south of the Huanglishan granodiorite pluton and has an exposure outcrop of ~2 km^2. The monzogranite generally shows a weak gneissosity. The constitute minerals include quartz (30–35%), alkali feldspar (35–40%), and plagioclase (25–30%), as well as several accessory phases of magnetite, zircon and apatite.

3. Analytical methods

3.1. In-situ zircon U–Pb and O isotopic analyses

Zircons were separated from the Jingshan and Huanglishan granodiorites and the Changhuaiwei granite using magnetic and heavy liquid separation methods, and then hand-picked under a binocular microscope. Approximately 100–200 grains for each sample, together with the zircon standard TEMORA2 (Black et al., 2004), were mounted into an epoxy resin disk. Prior to isotope analysis, all grains were photographed under both transmitted and reflected light, and subsequently examined using the cathodoluminescence (CL) image technique to reveal the internal structures of these zircon grains. Isotopic compositions were analyzed using a SHRIMP-II for Jingshan porphyry granodiorite sample 04JS-3 at the SHRIMP center (Beijing), in the Chinese Academy of Geological Sciences. Other samples were analyzed using a Cameca-IMS 1280 in the Institute of Geology and Geophysics, Chinese Academy of Science (IGGCAS), following the procedures outlined in Li et al. (2010). The spot size of an ion beam was ~30 μm. Measured Pb isotopic ratios were corrected for common Pb using the measured non-radiogenic ^{204}Pb. U–Pb ages were calculated using the ISOPLOT program of Ludwig (2001). In-situ zircon oxygen isotopic compositions were measured using the same Cameca-IMS 1280, and especially the analyzed spots were the same ones for the U–Pb analyses. Detailed procedures were shown in Li et al. (2009). Uncertainties on each analysis are at the 1σ level. Measured values of $\delta^{18}O$ are reported in standared per mil notation relative to VSMOW.

3.2. Ar–Ar isotopic analysis

Whole-rock samples of diabase were first crushed and sieved, and then the rock fractions (mesh 40–60) were selected by hand-picking, followed by washing in distilled water in an ultrasonic cleaner. Only fresh groundmass was separated from cleaned fractions. The groundmass samples were irradiated in a fast neutron flux at the Chinese Academy of Atomic Energy, Beijing. After three months, the irradiated samples were incrementally heated at the temperatures of 700–1500 °C by 18–20 steps in a high-vacuum argon extraction system at the Laboratory of Ar–Ar isotopic Dating in the IGGCAS. Then, the purified argon was analyzed on the VG-5400 gas mass spectrometer.

3.3. Major and trace elements

Major elements were analyzed using the wet-chemistry methods at the Langfang laboratory of Regional Geological Exploration Bureau of Hebei Province, China. Losses of ignition (LOI) were determined by gravimetric methods. Analytical uncertainties of major elements were better than 2% and for the majority were better than 1%. Trace element analyses were accomplished using an inductively coupled plasma mass spectrometer (ICP-MS) at the University of Science and Technology of China, similar to procedures described in Liu et al. (2010). The whole-rock powder (~50 mg) was dissolved in a mixture of $HF + HNO_3$ at 190 °C using Parr bombs for ~72 h, and complete sample dissolution was achieved. The dissolved samples were diluted to 50 ml using 1% HNO_3 before analysis. Reproducibility was better than 5% for elements with concentrations >10 ppm and less than 10% for those <10 ppm based on long-term analysis of standard materials.

3.4. Whole-rock Sr–Nd–Pb isotopic analyses

The Rb–Sr and Sm–Nd concentrations and isotopic ratios were determined using isotope dilution methods. Isotopic measurements were performed on a Finnigan MAT-262 thermal ionization mass

spectrometer (TIMS) at the IGGCAS. The mass fractionation corrections for Sr and Nd isotopic ratios were based on $^{86}Sr/^{88}Sr = 0.1194$ and $^{146}Nd/^{144}Nd = 0.7219$, respectively. Analyses of standards during the period of analysis were as follows: NBS987 of $^{87}Sr/^{86}Sr = 0.710248 \pm 12$ (2σ); and Jndi-1 of $^{143}Nd/^{144}Nd = 0.512112 \pm 12$ (2σ). For Pb isotopic measurement, whole-rock samples were dissolved in concentrated HF, and Pb was purified by cation-exchange technique. Isotopic ratios were measured with a Multi-Collector Inductively Coupled Plasma Mass Spectrometer (MC-ICP-MS) at the Institute of Geology, Chinese Academy of Geological Sciences. Thallium was added as an internal standard to correct instrumental mass discrimination. Long-term analysis of the NBS981 standard yielded $^{206}Pb/^{204}Pb = 16.940 \pm 0.010$ (±2σ), $^{207}Pb/^{204}Pb = 15.498 \pm 0.009$, and $^{208}Pb/^{204}Pb = 36.716 \pm 0.023$, respectively.

Table 1
SIMS zircon U–Pb elemental and isotopic compositions of Early Cretaceous granitoid rocks from the Bengbu area.

Sample	U	Th	Pb	$^{207}Pb/^{235}U$	±1σ	$^{206}Pb/^{238}U$	±1σ	$^{207}Pb/^{235}U$ age	±1σ	$^{206}Pb/^{238}U$ age	±1σ
Huanglishan granodiorite (HLS-1)											
Spot no.01	787	256	16	0.11073	3.11	0.0181	1.63	106.6	3.2	115.4	1.9
Spot no.02	98	93	40	4.30861	1.73	0.2996	1.50	1695	14.4	1689	22.4
Spot no.03	108	94	65	9.22520	1.62	0.4310	1.52	2360	14.9	2310	29.5
Spot no.04	171	214	4	0.11888	3.89	0.0180	1.58	114.1	4.2	115.0	1.8
Spot no.05	106	56	43	6.41702	1.78	0.3122	1.56	2035	15.8	1751	23.9
Spot no.06	295	113	6	0.11617	5.29	0.0180	1.50	111.6	5.6	115.3	1.7
Spot no.07	145	40	4	0.14260	6.59	0.0222	1.53	135.4	8.4	141.8	2.1
Spot no.08	205	86	4	0.11473	6.58	0.0181	1.56	110.3	6.9	115.8	1.8
Spot no.09	404	314	10	0.12600	3.27	0.0184	1.60	120.5	3.7	117.6	1.9
Spot no.10	112	117	63	8.06338	1.66	0.3931	1.51	2238	15.1	2137	27.5
Spot no.13	637	173	13	0.11336	3.43	0.0181	1.53	109.0	3.6	115.4	1.7
Spot no.14	388	110	8	0.12208	4.76	0.0182	1.83	117.0	5.3	116.1	2.1
Spot no.15	117	70	3	0.11308	8.79	0.0179	1.62	108.8	9.1	114.6	1.8
Spot no.16	24	50	10	3.62989	2.76	0.2448	1.53	1556	22.2	1412	19.5
Spot no.17	204	76	4	0.11384	6.20	0.0180	1.62	109.5	6.5	115.1	1.9
Spot no.18	489	139	10	0.11452	4.45	0.0183	1.51	110.1	4.7	116.9	1.8
Spot no.19	130	38	3	0.09578	12.89	0.0177	1.70	92.9	11.5	113.3	1.9
Spot no.20	392	128	8	0.12093	5.14	0.0174	1.75	115.9	5.6	111.3	1.9
Spot no.21	99	27	2	0.12605	6.86	0.0181	2.07	120.5	7.8	115.8	2.4
Spot no.22	161	57	3	0.11603	6.47	0.0171	2.14	111.5	6.9	109.3	2.3
Spot no.23	22	6	14	12.32359	1.94	0.4928	1.56	2629	18.4	2583	33.2
Spot no.24	137	55	3	0.09323	10.15	0.0178	1.68	90.5	8.8	113.9	1.9
Spot no.25	952	728	23	0.12469	2.23	0.0183	1.51	119.3	2.5	116.9	1.8
Spot no.27	705	280	15	0.11369	2.66	0.0181	1.51	109.3	2.8	115.9	1.7
Spot no.29	170	135	4	0.11159	5.41	0.0178	1.59	107.4	5.5	113.8	1.8
Spot no.30	1159	447	24	0.12075	2.09	0.0179	1.51	115.8	2.3	114.7	1.7
Spot no.31	145	58	3	0.12677	4.74	0.0183	1.62	121.2	5.4	116.7	1.9
Spot no.33	394	303	9	0.11515	4.63	0.0181	1.50	110.7	4.9	115.9	1.7
Spot no.34	1043	310	21	0.11937	2.19	0.0180	1.54	114.5	2.4	115.2	1.8
Spot no.35	473	110	9	0.11533	3.33	0.0179	1.59	110.8	3.5	114.4	1.8
Spot no.36	233	93	5	0.11544	4.49	0.0183	1.75	110.9	4.7	117.0	2.0
Jingshan granodiorite (JS-5)											
Spot no.01	622	112	13	0.12133	3.21	0.0189	1.52	116.3	3.5	120.9	1.8
Spot no.02	1561	111	31	0.12497	2.04	0.0187	1.50	119.6	2.3	119.5	1.8
Spot no.03	228	39	5	0.12572	4.49	0.0201	1.50	120.2	5.1	128.5	1.9
Spot no.04	2671	328	54	0.12468	2.22	0.0188	1.52	119.3	2.5	119.8	1.8
Spot no.05	567	846	16	0.11721	2.81	0.0185	1.53	112.5	3.0	118.2	1.8
Spot no.06	1935	300	40	0.12404	1.88	0.0188	1.51	118.7	2.1	119.9	1.8
Spot no.07	522	100	10	0.11883	10.22	0.0182	1.60	114.0	11.1	116.5	1.8
Spot no.08	1040	255	22	0.12162	1.99	0.01850	1.50	116.5	2.2	118.1	1.8
Spot no.09	793	422	18	0.12132	2.15	0.01831	1.51	116.3	2.4	117.0	1.7
Spot no.10	763	293	17	0.12147	2.27	0.01861	1.51	116.4	2.5	118.8	1.8
Spot no.13	756	231	16	0.12196	2.30	0.01834	1.54	116.8	2.5	117.2	1.8
Spot no.14	603	151	13	0.12413	2.71	0.01836	1.51	118.8	3.0	117.3	1.8
Spot no.15	696	204	15	0.12107	2.61	0.01836	1.55	116.0	2.9	117.3	1.8
Spot no.16	332	78.4	6.8	0.12547	2.61	0.01812	1.51	120.0	3.0	115.8	1.7
Spot no.17	496	664	13	0.11817	3.00	0.01829	1.51	113.4	3.2	116.8	1.7
Spot no.18	704	230	15	0.12256	2.24	0.01841	1.51	117.4	2.5	117.6	1.8
Spot no.19	898	233	19	0.12331	2.13	0.01853	1.51	118.1	2.4	118.4	1.8
Spot no.20	463	89.7	9.4	0.11848	2.59	0.01839	1.53	113.7	2.8	117.5	1.8
Spot no.21	1393	56.7	526	5.28985	1.52	0.33548	1.50	1867.2	13.1	1865	24.4
Changhuaiwei Granite (CHW-1)											
Spot no.01	1379	411	27.9	0.11887	2.83	0.01778	1.50	114.1	3.1	113.6	1.7
Spot no.02	997	489	21.1	0.11213	2.92	0.01769	1.50	107.9	3.0	113.0	1.7
Spot no.03	239	131	4.8	0.12301	4.52	0.01707	1.59	117.8	5.0	109.1	1.7
Spot no.04	492	171	9.9	0.11128	3.34	0.01743	1.67	107.1	3.4	111.4	1.8
Spot no.05	509	278	9.0	0.10383	8.05	0.01523	1.55	100.3	7.7	97.5	1.5
Spot no.06	246	87	4.9	0.11396	4.25	0.01727	1.63	109.6	4.4	110.4	1.8
Spot no.07	1112	531	23.6	0.11704	2.20	0.01775	1.54	112.4	2.3	113.4	1.7
Spot no.08	387	154	8.2	0.12059	3.52	0.01804	1.52	115.6	3.9	115.3	1.7
Spot no.09	998	317	20.1	0.11599	2.42	0.01753	1.51	111.4	2.6	112.0	1.7
Spot no.10	1043	272	20.8	0.11364	2.51	0.01759	1.61	109.3	2.6	112.4	1.8

4. Results

4.1. Zircon U–Pb ages of granitoids

Zircon U–Th–Pb elemental and isotopic data are reported in Table 1 and Supplementary Tables A1 and A2. The U–Pb concordia diagrams and representative CL images of zircons are given in Fig. 2a–f. CL images show that zircons from these samples are generally euhedral and occasionally contain inherited cores surrounded by prismatic and transparent rims. The rims generally have high Th/U further indicating magmatic origin. Analyses of the zircon rims from the Jingshan granodiorite (JS-5) yielded a weighted mean $^{206}Pb/^{238}U$ age of 118 ± 1 Ma (n = 23; MSWD = 0.66) (Fig. 2a). A single analysis of one of the cores falls on the concordia line with a $^{207}Pb/^{235}U$ age of 1867 ± 13 Ma. In addition, four SHRIMP spot analyses of the zircon rims (Fig. 2b) from the Jingshan porphyry granodiorite (04JS-3) gave a weighted mean age of 123.1 ± 3.5 Ma and a single analysis of a zircon core yielded an age of 1869 ± 32 Ma, which are consistent with the dating results of granodiorite sample JS-5 within errors.

SIMS analytical results of the Huanglishan granodiorite (HLS-1) yielded a weighted mean $^{206}Pb/^{238}U$ age of 115 ± 1 Ma (n = 21; MSWD = 0.65) (Fig. 2c). The inherited cores have a wide variation of $^{207}Pb/^{235}U$ ages ranging from 1556 to 2629 Ma, with some deviated from the concordant line as a result of variable extents of Pb loss. To further confirm the accuracy of our SIMS ages, we analyzed zircons from the same sample using the laser ablation-ICP-MS technique (Supplementary Table A1). The laser ablation-ICP-MS analysis yielded a weighted mean $^{206}Pb/^{238}U$ age of 118 ± 3 Ma (n = 12; MSWD = 4.0) (Fig. 2d). This is in agreement within errors with the SIMS ages despite being slightly more scattered. Additionally, the laser ablation-ICP-MS analysis generated similar $^{207}Pb/^{235}U$ ages of inherited zircons ranging from 1700 to 2733 Ma, with the concordia ages predominantly dated ~1.8 Ga and ~2.5 Ga. Zircons from the Changhuaiwei granite (CHW-1) gave a weighted mean $^{206}Pb/^{238}U$ age of 112 ± 1 Ma (n = 9; MSWD = 1.12) (Fig. 2e) obtained using SIMS, which is significantly younger than the Jingshan and Huanglishan granodiorites.

4.2. Ar–Ar age of mafic dyke

Ar–Ar isotopic data of the Jingshan diabase dyke are provided in Supplementary Table A3, and the $^{40}Ar/^{39}Ar$ spectra with a plateau age and an

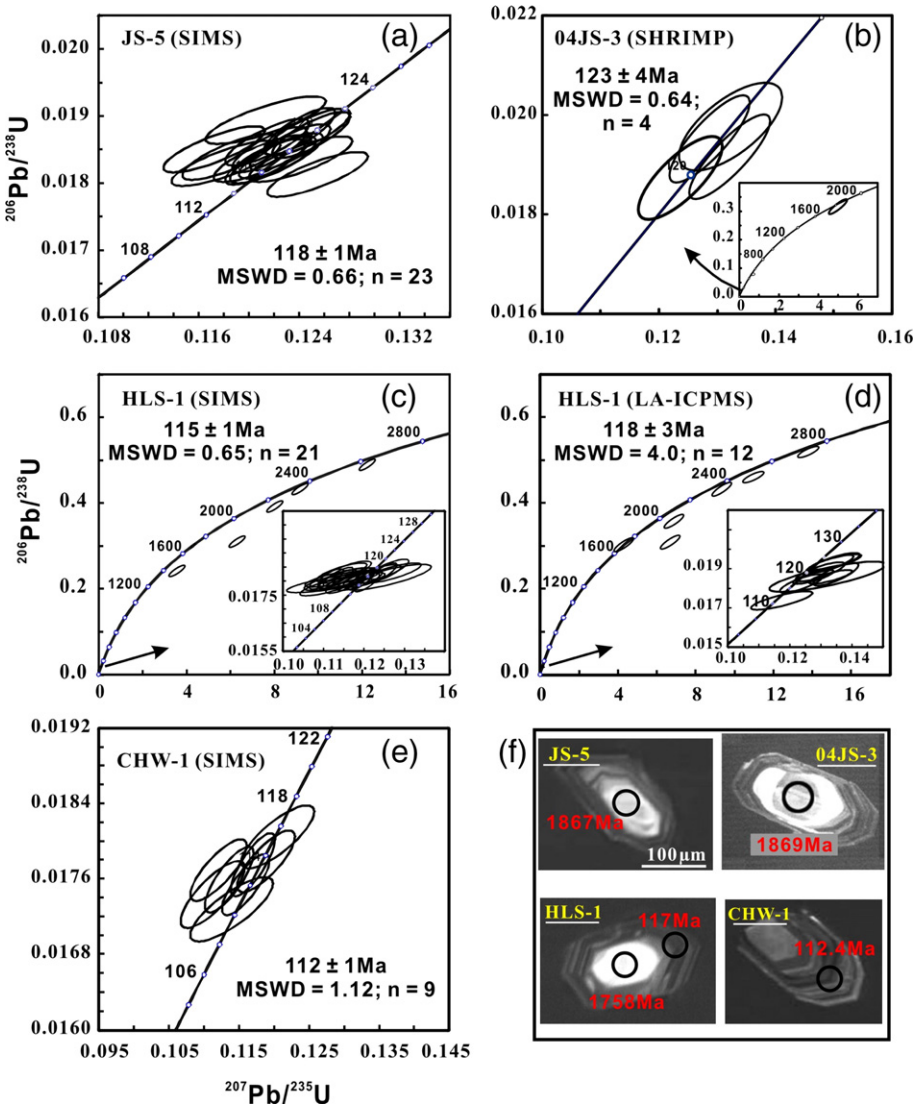

Fig. 2. Zircon U–Pb concordia diagrams and CL images for Mesozoic granitoids from the Bengbu area. (a) SIMS results of Jingshan granodiorites (JS-5), (b) SHRIMP results of Jingshan porphyry granodiorite (04JS-3), (c) SIMS results of Huanglishan granodiorite (HLS-1), (d) LA-ICP-MS results of Huanglishan granodiorite (HLS-1), (e) SIMS results of Changhuaiwei monzogranite (CHW-1), and (f) representative CL images of the dated zircon grains. Data are reported in Table 1 and Supplementary Tables A1 and A2. The errors of U–Pb ages denote 1σ uncertainties.

isochron are plotted in Fig. 3a–b. The analytical results yielded a $^{40}Ar/^{39}Ar$ plateau with age of 111.8 ± 0.6 Ma, which is defined by 78% of total released ^{39}Ar. The isochron gave an age of 109.6 ± 1.5 Ma identical to the plateau age. This isochron defines an initial $^{40}Ar/^{36}Ar$ ratio of 334 ± 40 (2σ), which is consistent with the present atmosphere value (296) within error, implying that the possible effect of excess argon on the obtained plateau age is insignificant.

4.3. Chemical compositions of granitoids and mafic dykes

4.3.1. Granitoid rocks

Chemical compositions of the granitoids and mafic dykes are reported in Table 2. The Jingshan and Huanglishan granodiorites have similar compositions of major oxides, with SiO_2 varying from 69.1 to 72.5 wt.%, MgO from 0.43 to 1.0 wt.%, and Mg# from 30.7 to 47.6. They are enriched in total alkali ($K_2O + Na_2O$ = 7.23 to 9.54 wt.%), and have ratios of K_2O/Na_2O ranging from 0.8 to 1.1. Three granodiorite samples from the Huaiguang intrusion (130 Ma) in the Bengbu area reported in Yang et al. (2010) show major elemental compositions that fall within the ranges of the Huanglishan and Jingshan granodiorites studied here (Fig. 5). Compared to the Bengbu granodiorites, the Changhuaiwei monzogranites have more felsic compositions with SiO_2 of 74.4–75.0 wt.%, lower Al_2O_3 and CaO, but similar MgO and total alkali contents (Fig. 5). The metaluminous to weakly peraluminous features [A/CNK = molar $Al_2O_3/(CaO + Na_2O + K_2O)$ = 1.02–1.23] indicate an igneous protolith for these granitoids.

The Bengbu granodiorites and granites are all enriched in large ion lithophile elements (LILEs) and depleted in high field strength elements (HFSEs), with negative anomalies of Nb, Ta and Ti, and positive anomalies of Pb (Fig. 6d). However, the granitoids display more prominent light rare earth elements (LREE) enrichment and heavy rare earth elements (HREE) depletion ($(La/Yb)_N$ = 39.7 to 58.4) relative to the granites ($(La/Yb)_N$ = 12.0 to 17.3) (Fig. 6b), and the granodiorites show slightly positive Eu anomalies while the granites show prominently negative Eu anomalies. In addition, the granodiorites possess much higher Sr and lower Y and Yb contents than the granites, which are similar to those of adakitic rocks (Fig. 7). In particular, the granodiorites show fractionated $(Dy/Yb)_N$ (1.26–1.71), which are coupled with high $(La/Yb)_N$ values, whereas the granites show almost non-fractionated $(Dy/Yb)_N$ values close to unit (1.05–1.16).

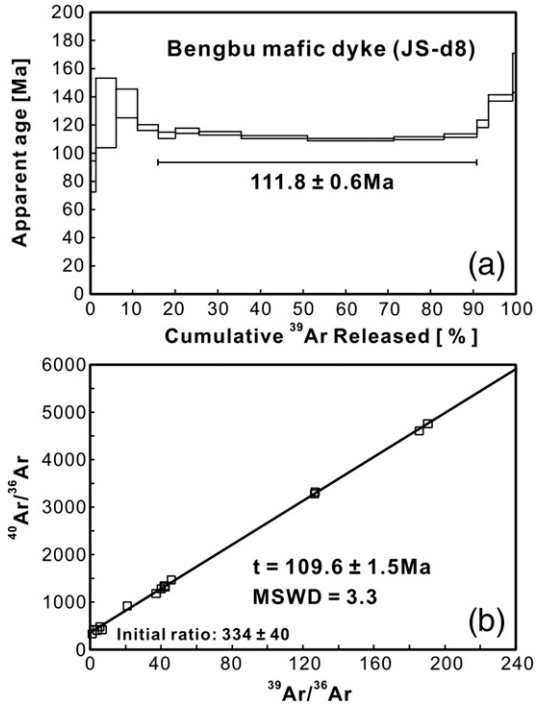

Fig. 3. Whole-rock ^{40}Ar–^{39}Ar age spectrum (a) and isochron plots (b) for mafic dyke (JS-d8) from Jingshan in the Bengbu area. Data are reported in Supplementary Table A3.

4.3.2. Mafic rocks

The Bengbu mafic dykes have SiO_2 contents varying between 42.1 and 49.9 wt.%. They are enriched in total alkali ($K_2O + Na_2O$ = 3.75 to 6.17 wt.%) and fall in the field of alkaline basaltic rocks series (Fig. 4). They have relatively low MgO contents of 4.50–8.68 wt.%, Mg# of 45.4–62.9, Cr (76–136 ppm) and Ni (66.1–130 ppm), implying a moderate extent of fractional crystallization of mafic minerals, e.g. olivine and/or pyroxene. The correlations of SiO_2 with MgO and Al_2O_3 (Fig. 5a, b) are consistent with fractional crystallization of olivines during magmatic evolution. There is no clear correlation between SiO_2 and total FeO (Fig. 5c) and between SiO_2 and CaO (Fig. 5d) for most samples.

The chondrite-normalized REE patterns of the Bengbu mafic rocks display significant enrichment of LREEs relative to HREEs with $(La/Yb)_N$ greater than 10, distinctly different from typical mid-ocean ridge basalts (N-MORB) (Fig. 6b). In primitive-mantle normalized incompatible element diagrams (Fig. 6d), these rocks are characterized by remarkable enrichment of LILEs and Pb, and in particular, depletion of Nb, Ta, Zr, Hf and Ti (Fig. 6). These trace element features are similar to those of Mesozoic mafic intrusions/lavas from other areas in the NCC (e.g., Chen et al., 2004; Guo et al., 2001; Yang and Li, 2008; Zhang et al., 2002) but different from those of MORB and OIB. In addition, they have lower Nb/U (13.7–14.3), Ce/Pb (9.8–31.0), Nb/Ta (16.3–18.5), higher La/Nb (2.6–3.1) and Ba/Nb (40.3–59.8) than the primitive mantle and the OIB (e.g., Fig. 8b). Although such features are quite common in Mesozoic mafic igneous rocks from the NCC, they do not exist in Cenozoic alkaline basalts from the NCC which generally have OIB-like elemental and isotopic signatures (e.g., Chen et al., 2007; Tang et al., 2006; Zhi et al., 1990; Zou et al., 2000). This suggests that Mesozoic and Cenozoic basaltic rocks in the NCC sampled different magma source regions and had distinct origins.

4.4. Sr, Nd and Pb isotopes of granitoids and mafic rocks

Initial Sr, Nd and Pb isotopic data of granitoids and mafic rocks are reported in Table 3 and plotted in Figs. 9 and 10, respectively. Initial isotopic ratios were calculated back to 112 Ma. The Jingshan granodiorites have initial $^{87}Sr/^{86}Sr$ = 0.70903 to 0.70926 and εNd (t) = −19.4 to −18.5. The Huanglishan granodiorites have slightly lower initial $^{87}Sr/^{86}Sr$ (0.70752 to 0.70823) and more negative (depleted) εNd (t) values (−21.7 to −19.4) relative to the Jingshan granodiorites. The mafic rocks in the Bengbu area have relatively uniform εNd (t) values (−6.1 to −5.8) but slightly variable initial $^{87}Sr/^{86}Sr$ of 0.70641 to 0.70816.

The Jingshan granodiorites show unradiogenic Pb isotopic compositions with $^{206}Pb/^{204}Pb$ (t) = 17.015–17.017, $^{207}Pb/^{204}Pb$ (t) = 15.438 (n = 2), and $^{208}Pb/^{204}Pb$ (t) = 37.57 (n = 2). The Huanglishan granodiorites have slightly less radiogenic Pb with $^{206}Pb/^{204}Pb$ (t) = 16.524–16.636, $^{207}Pb/^{204}Pb$ (t) = 15.331 to 15.374, and $^{208}Pb/^{204}Pb$ (t) = 37.047 to 37.189. The mafic rocks also have low radiogenic Pb isotopic characteristics, with $^{206}Pb/^{204}Pb$ (t) = 16.782–17.262, $^{207}Pb/^{204}Pb$ (t) = 15.384 to 15.429, and $^{208}Pb/^{204}Pb$ (t) = 37.197 to 37.738, which are similar to those of Mesozoic basaltic rocks from Luxi and Jiaodong areas in the NCC (Fig. 10).

4.5. In-situ zircon Hf–O isotopic compositions of granitoids

In-situ Hf and O isotopic data of zircons from the Bengbu granitoids are reported in Table 4 and the evolution of Hf isotopic

Table 2
Compositions of major oxides and trace elements of granitoid and mafic dykes from the Bengbu area.

Location	Jingshan granodiorite							Huanglishan granodiorite						
Sample	JS-1	JS-3	JS-4	JS-5	JS-9	JS-11	JS-12	HLS01	HLS02	HLS-1	HLS-2	HLS-3	HLS-4	HLS-9
SiO_2	69.14	71.68	72.02	71.94	72.06	72.24	72.42	70.58	71.20	70.36	71.12	70.14	69.88	72.53
Al_2O_3	15.07	15.17	14.61	14.91	14.68	14.67	14.96	14.83	14.76	15.48	15.39	15.25	15.79	14.86
TiO_2	0.18	0.17	0.18	0.17	0.16	0.17	0.17	0.19	0.17	0.26	0.17	0.28	0.26	0.16
Fe_2O_3	0.80	1.52	0.66	0.81	0.57	0.42	0.50	1.11	0.82	1.02	0.69	1.01	1.00	0.72
FeO	0.86	nd	0.69	0.67	0.81	0.77	0.76	0.98	1.01	1.17	0.86	1.29	1.22	0.82
CaO	1.99	1.75	1.69	1.99	1.82	1.82	1.74	2.38	2.48	2.73	2.53	2.65	2.85	2.17
MgO	0.43	0.48	0.43	0.43	0.43	0.43	0.44	1.00	0.43	0.82	0.50	0.84	0.80	0.52
K_2O	5.02	3.81	4.07	4.11	3.84	3.84	3.87	4.00	3.74	3.33	3.62	3.29	3.22	3.59
Na_2O	4.54	4.43	4.46	4.46	4.20	4.20	4.28	4.15	4.27	4.05	4.28	4.13	4.13	4.01
MnO	0.01	0.02	0.02	0.02	0.03	0.02	0.02	0.03	0.03	0.04	0.03	0.03	0.03	0.03
P_2O_5	0.07	0.06	0.08	0.07	0.07	0.07	0.07	0.07	0.08	0.09	0.05	0.09	0.10	0.07
LIO	1.18	0.57	0.30	0.35	0.41	0.38	0.40	0.46	0.44	0.53	0.26	0.45	0.49	0.42
Total	99.29	99.66	99.21	99.94	99.08	99.03	99.64	99.78	99.43	99.89	99.51	99.45	99.77	99.89
A/CNK	1.02	1.17	1.10	1.10	1.15	1.15	1.17	1.11	1.11	1.21	1.16	1.19	1.23	1.19
Mg#	32.9	38.7	37.6	35.6	36.9	40.3	39.6	47.6	30.7	41.4	37.8	40.7	40.4	38.9
Cr	13.3	5.37	13.6	7.88	3.39	5.82	3.13	6	13.9	7.37	3.99	636	7.44	3.18
Ni	6.37	2.45	2.37	3.43	2.36	2.41	1.3	4.07	7.33	4.67	2.73	221	4.77	2.51
Rb	105	114	111	126	114	120	120	92.5	91.5	96.7	99.2	85.4	89.4	96.5
Sr	781	535	554	594	570	560	570	587	596	606	562	639	685	498
Y	7.95	6.99	5.61	6.19	5.54	5.64	5.64	5.00	5.48	7.44	6.03	6.05	5.58	5.08
Zr	175	145.6	143	151	135	133	134	86.7	102	163	120	158	154	92.7
Nb	9.78	9.44	9.27	9.61	8.86	8.94	8.9	6.14	6.53	8.58	6.97	6.48	6.14	1.97
Cs	1.41	2.02	1.22	1.53	1.33	1.46	1.39	2.29	2.39	2.92	1.72	2.97	2.05	2.87
Ba	2202	1993	1865	2100	1962	1950	1960	2749	2427	2599	2366	2486	2629	2627
La	42.2	31.2	30.3	33.2	31.8	30.7	31	28.2	33.9	43.2	38.2	47.2	36.6	27.1
Ce	67.8	50.6	47.5	52.2	52.5	49.7	50.6	46.4	55.5	70.2	61.9	75	59.3	44.7
Pr	6.78	4.97	4.83	5.17	4.99	4.86	4.88	4.49	5.3	6.6	5.79	7.05	5.54	4.45
Nd	23.2	17.3	16.5	17.5	17.1	16.7	16.8	15.4	18.0	22.1	19.2	23.3	18.6	15.3
Sm	3.31	2.59	2.36	2.5	2.49	2.45	2.45	2.12	2.34	3	2.57	2.93	2.48	2.14
Eu	0.86	0.72	0.63	0.64	0.71	0.7	0.71	0.75	0.77	0.83	0.81	0.85	0.86	0.61
Gd	2.02	2.03	1.44	1.47	1.89	1.87	1.87	1.32	1.48	2.34	2	2.24	1.93	1.61
Tb	0.25	0.24	0.18	0.19	0.21	0.21	0.22	0.16	0.18	0.27	0.22	0.24	0.21	0.18
Dy	1.44	1.13	1.05	1.10	1.03	1.06	1.05	0.90	0.98	1.38	1.13	1.15	1.05	0.92
Ho	0.24	0.21	0.17	0.17	0.17	0.17	0.17	0.16	0.18	0.24	0.2	0.2	0.18	0.16
Er	0.58	0.53	0.43	0.46	0.45	0.49	0.47	0.42	0.45	0.71	0.57	0.57	0.51	0.47
Tm	0.09	0.08	0.06	0.06	0.07	0.07	0.07	0.07	0.07	0.1	0.08	0.08	0.07	0.07
Yb	0.63	0.51	0.41	0.43	0.43	0.47	0.45	0.44	0.48	0.72	0.55	0.58	0.51	0.49
Lu	0.09	0.08	0.06	0.06	0.07	0.07	0.07	0.07	0.08	0.11	0.08	0.09	0.08	0.08
Hf	3.60	3.58	3.38	3.53	3.51	3.48	3.49	2.08	2.39	4.02	3.01	3.7	3.59	2.54
Ta	0.70	0.80	0.80	0.83	0.79	0.81	0.8	0.42	0.47	0.71	0.5	0.56	0.41	0.14
Pb	34.4	44.5	44.2	49.3	46.2	46.9	46.2	39.8	39.1	40.9	48.1	39	41.3	46.8
Th	11.0	9.95	7.73	8.20	8.3	8.09	8.07	5.73	6.29	10	8.09	6.44	6.13	7.26
U	2.07	3.01	2.86	2.88	2.75	2.76	2.8	2.04	1.89	1.71	1.13	1.19	1.11	1.55
Sr/Y	98.2	76.6	98.8	96.0	102.9	99.3	101.1	117.4	108.8	81.5	93.2	105.6	122.8	98.0
$(La/Yb)_N$	48.0	43.8	53.0	55.4	53.0	46.9	49.4	46.0	50.7	43.0	49.8	58.4	51.5	39.7
$(Dy/Yb)_N$	1.53	1.48	1.71	1.71	1.60	1.51	1.56	1.37	1.37	1.28	1.38	1.33	1.38	1.26

Location	Changhuaiwei granite		Bengbu mafic dykes								
Sample	CHW-1	CHW-3	04JS-d1	04JS-d2	04JS-d3	JS-d1	JS-d2	JS-d6	JS-d7	JS-d8	HLS-d3
SiO_2	75.02	74.40	44.20	44.80	45.70	42.12	43.08	44.96	43.62	45.18	49.9
Al_2O_3	13.20	13.10	15.69	15.48	16.18	14.68	14.9	16.08	15.02	16.16	17.18
TiO_2	0.09	0.12	1.76	1.80	1.31	1.29	1.40	1.48	1.65	1.45	1.78
Fe_2O_3	0.55	0.58	3.46	3.46	3.79	3.29	3.8	3.32	3.18	2.85	3.80
FeO	0.48	0.60	6.28	6.59	6.75	6.37	6.25	6.63	6.44	6.85	6.34
CaO	1.07	1.15	10.56	10.86	10.18	11.15	10.45	10.8	10.10	11.07	7.55
MgO	0.43	0.43	7.86	7.50	7.32	8.15	8.68	7.73	8.77	7.43	4.50
K_2O	4.56	4.37	2.56	1.99	1.18	1.54	1.21	1.75	0.93	1.44	2.36
Na_2O	4.04	4.15	2.48	2.79	3.06	2.55	2.95	2.76	2.82	3.1	3.81
MnO	0.03	0.05	0.18	0.18	0.20	0.16	0.16	0.20	0.17	0.19	0.15
P_2O_5	0.13	0.05	0.65	0.70	0.59	0.52	0.58	0.74	0.64	0.63	0.88
H_2O^+	0.31	0.10	1.20	0.91	1.92	2.72	2.65	1.07	3.30	1.31	0.74
H_2O^-	0.18	0.16	0.32	0.22	0.19	0.27	0.32	0.21	0.28	0.27	0.15
LIO	0.41	0.44	3.73	2.99	3.16	7.38	5.81	2.84	6.21	3.27	1.42
Total	100.0	99.44	99.41	99.50	99.42	99.2	99.27	99.28	99.54	99.63	99.67
Mg#	44.3	40.8	60.1	58.2	56.5	61.1	61.8	59.1	62.9	58.7	45.4
Cr	1.81	8.23	92	88	84	139	132	76	163	82	98
Ni	1.15	26.5	87.3	86.6	67.4	97.8	96	66.9	130	70.2	66.1
Rb	198	190	102.6	62.5	32.9	62.9	50	57.7	41.18	46	45.7
Sr	150	142	852	914	990	692	731	963	891	943	877
Y	13.9	9.57	29.8	30.4	28.8	26	26.3	30.3	28	28.1	29.2
Zr	78.6	109	166	167	177	146	149	172	149.2	171	176
Nb	22.2	17.5	20.3	20.1	21.3	16.5	17.3	20.2	17.7	20	21.4

(continued on next page)

Table 2 (*continued*)

Location	Changhuaiwei granite		Bengbu mafic dykes								
Sample	CHW-1	CHW-3	04JS-d1	04JS-d2	04JS-d3	JS-d1	JS-d2	JS-d6	JS-d7	JS-d8	HLS-d3
Cs	2.58	3.28	4.78	5.60	1.53	4.28	2.57	4.5	1.76	3.1	2.35
Ba	483	443	1179	1204	1230	839	788	1186	711	1169	1101
La	22.0	19.8	56.0	56.0	56.9	50.8	52.0	58.7	50.9	53.7	56.2
Ce	39.8	36.1	114	116	119	108	110	124	107	113	118
Pr	4.22	3.88	13.8	14.0	13.6	12.6	12.8	14.4	13.0	13.0	13.7
Nd	15.2	13.8	56.9	58.1	56.1	53.4	53.7	59.9	54.7	54.1	56.5
Sm	2.88	2.54	10.00	10.22	9.84	9.51	9.55	10.60	9.74	9.69	9.99
Eu	0.41	0.36	2.94	2.83	2.75	2.55	2.50	2.90	2.62	2.69	2.71
Gd	2.28	1.66	8.23	8.48	7.61	7.28	7.31	8.32	7.96	7.49	7.87
Tb	0.34	0.23	1.06	1.09	1.02	0.96	0.97	1.10	1.03	1.01	1.04
Dy	2.08	1.42	5.65	5.84	5.33	4.98	5.01	5.87	5.42	5.26	5.59
Ho	0.40	0.25	1.11	1.14	1.02	0.93	0.93	1.07	1.04	1.00	1.03
Er	1.10	0.70	2.87	2.96	2.82	2.56	2.56	2.94	2.61	2.73	2.83
Tm	0.19	0.11	0.39	0.40	0.39	0.35	0.35	0.42	0.36	0.38	0.40
Yb	1.32	0.82	2.59	2.63	2.58	2.24	2.26	2.67	2.33	2.49	2.62
Lu	0.21	0.13	0.38	0.39	0.39	0.33	0.33	0.39	0.35	0.37	0.39
Hf	2.90	3.43	3.39	3.44	3.42	3.00	3.03	3.41	3.17	3.33	3.48
Ta	2.22	1.23	1.22	1.21	1.15	0.91	0.95	1.12	1.08	1.10	1.17
Pb	70.6	58.8	11.72	4.54	4.28	3.48	5.66	4.25	6.07	4.48	10.50
Th	19.3	16.8	7.20	7.01	7.77	5.84	6.17	7.09	6.25	7.05	7.24
U	6.67	5.95	1.48	1.46	1.49	1.19	1.24	1.45	1.29	1.45	1.55
Nb/U	3.33	2.94	13.8	13.8	14.3	13.9	14.0	13.9	13.7	13.8	13.8
Ce/Pb	0.56	0.61	9.8	25.5	27.8	31.0	19.4	29.2	17.6	25.2	11.2

Notes: Major elements are normalized to 100% on a volatile-free basis. A/CNK is the molar ratio of $Al_2O_3/(CaO+Na_2O+K_2O)$. Mg# = 100 × molar Mg/(Mg + total Fe^{2+}). The chondrite normalized values are from Sun and McDonough (1989).

compositions with time is plotted in Fig. 11. The Huanglishan and Jingshan granodiorites and the Changhuaiwei granites gave a narrow range of $\delta^{18}O_{zircon}$ values: 4.91–6.39‰ (mean = 5.91 ± 0.17‰; n = 14; 1σ), 5.10–5.90‰ (mean = 5.83 ± 0.19‰; n = 9; 1σ), and 5.12–6.18‰ (mean = 5.79 ± 0.18‰; n = 6; 1σ), respectively. Inherited zircons of Late Archean to Paleoproterozoic ages from the Huanglishan granodiorite have $\delta^{18}O_{zircon}$ values between 5.22 and 6.79‰, similar to values of magmatic zircons of the host granitoids. The εHf (112 Ma) values of the Huanglishan granodiorites vary from −21.4 to −16.5 with corresponding two-stage "depleted mantle" model ages (T_{DM2}) ranging from 1.80 to 2.14 Ga. The Changhuaiwei granites have εHf (112 Ma) of −22.8 to −16.4. The model T_{DM2} ages vary from 1.82 to 2.22 Ga.

5. Discussion

5.1. Temporal sequence of Early Cretaceous magmatism in the Bengbu area

The geochronological data obtained in this study and reported in previous work are summarized in Table 5, which allow recognition of a characteristic formation sequence of various types of igneous rocks in the Bengbu area. Although whole-rock Ar–Ar ages of plutons commonly record the time since the magmas cooled down below the closure temperature, the rapid cooling of diabasic magmas indicates that the Ar–Ar ages are close to the time of intrusion, especially considering that the Ar–Ar plateau age (162.8 ± 0.3 Ma) for biotite from the Bengbu Jurassic leucogranites suggests that the country rocks of the diabase dykes had been cooled down to 300 °C at Late Jurassic (Qiu et al., 1999). Thus we compared the diabase Ar–Ar ages with the granitoid zircon U–Pb ages directly. The compiled data reveal that granodiorites, monzogranites and mafic dykes in the Bengbu area were emplaced during the Early Cretaceous within a relatively short time period (≤18 Ma).

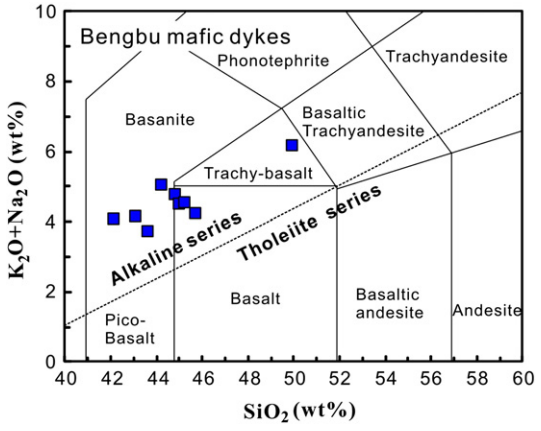

Fig. 4. $K_2O + Na_2O$ vs. SiO_2 classification diagrams for Mesozoic mafic rocks from the Bengbu area. The dotted line represents the boundary of alkaline and tholeiite series following the chemical classification of Irvine and Babagar (1971).

In details, the granodiorites were formed before ~115 Ma (Huanglishan and Jingshan plutons; this study), and probably as early as at 130 Ma (Huaiguang pluton) (Yang et al., 2010). They are significantly older than the monzogranites from the Changhuaiwei pluton (112 Ma; this study) and also the Caoshan pluton (112 Ma) (Yang et al., 2010) in the Bengbu area. The Jingshan mafic dykes were emplaced almost at the same time of the Bengbu monzogranites (~112 Ma), and both are significantly younger than the Jingshan granodiorite (118 Ma). In the Huanglishan, although the exact emplacement age of the mafic dykes is unknown, it must be formed later than the granodiorite because field-based observation indicates that the dykes cut across the granodiorite pluton. Overall, geochronological data indicate that granodiorites were formed prior to mafic dykes and monzogranites in the Bengbu area.

5.2. Petrogenesis of granitoids in the Bengbu area

5.2.1. Partial melting of a thickened LCC or a shallow crust?

The Jingshan and Huanglishan granitoids studied in this study and the Huaiguang granodiorites reported in Yang et al. (2010) are characterized by high Sr, low Y contents, and high Sr/Y and La/Yb ratios (Fig. 7). These features resemble those of adakites defined in Defant and Drummond (1990), and can be applied to place constraints on the pressures at which magmas originated, e.g., in the stability field of garnet or not. Recent studies, however, show that such features may be produced through multiple mechanisms (see review of Moyen, 2009). These include high-pressure fractional crystallization

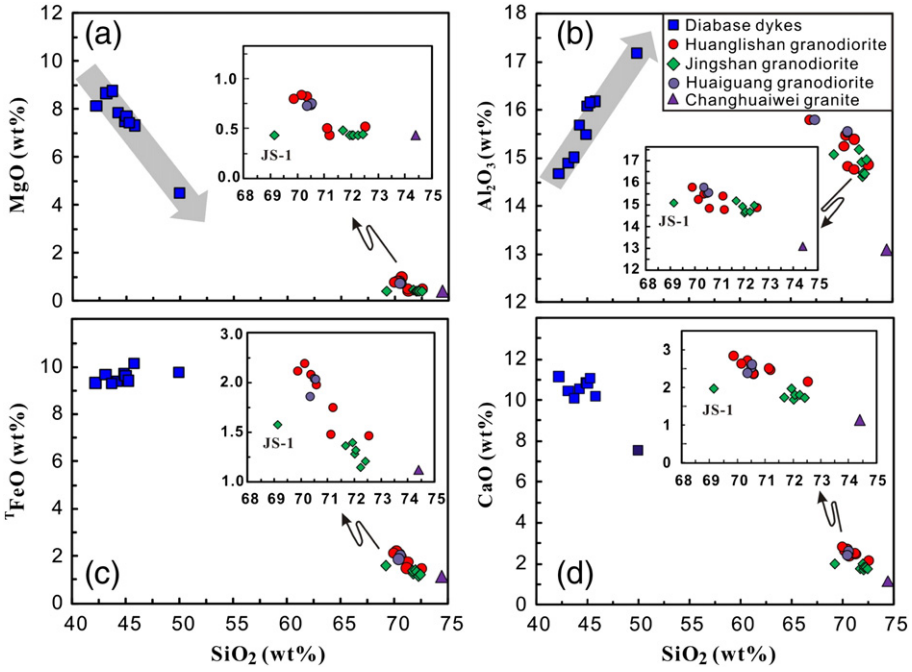

Fig. 5. Variations of major oxides with SiO_2 for granitoids and mafic rocks from the Bengbu area. (a) MgO vs. SiO_2; (b) Al_2O_3 vs. SiO_2; (c) total FeO vs. SiO_2; (d) CaO vs. SiO_2. Data of the Huaiguang granodiorites are from Yang et al. (2010).

of mafic minerals from basaltic magmas (Castillo et al., 1999; Macpherson et al., 2006), partial melting of high Sr/Y source (Kamei et al., 2009), and the original model of high-pressure melting of basalts in the garnet stability field (Defant and Drummond, 1990; Martin et al., 2005). Apart from radiogenic isotope systems, chemical parameters that may effectively discriminate these petrogenetic mechanisms were outlined in a recent study of post-collisional granitoids from the Dabie Orogen (He et al., 2011). These include that rocks formed in garnet stability and plagioclase-free fields (low-Mg# adakitic rocks) should have high Sr contents for a given SiO_2 or CaO, low Nb/Ta, and positive correlations between Sr/Y, $(La/Yb)_N$ and $(Dy/Yb)_N$, when compared to those formed in garnet-free field (normal granitoids). Although plagioclase remains a stable phase at pressures up to 3.0 GPa (Patino Douce, 2005; Skjerlie and Johnston, 1996), the lacking of Eu anomalies and high Sr contents in the adakitic rocks imply little plagioclase in the residues. In particular, the high $(Dy/Yb)_N$ and its positive correlation with $(La/Yb)_N$ require the dominate role of garnet during partial melting, the only rock-forming mineral that can substantially fractionate the HREE (e.g., Klein et al., 2000; Pertermann et al., 2004).

As illustrated in Fig. 7, the Bengbu granodiorites have chemical features similar to those of the Dabie low-Mg# adakitic rocks. For

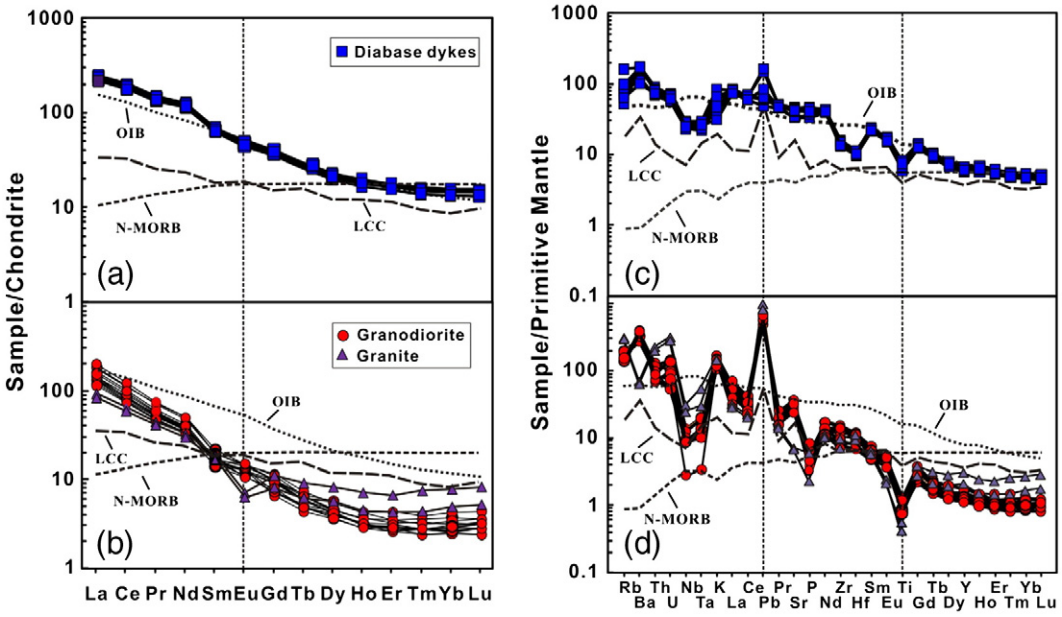

Fig. 6. Chondrite-normalized rare earth element (REE) patterns (a and b) and primitive mantle-normalized trace element patterns (c and d) for Mesozoic mafic rocks and granitoids from the Bengbu area.
Compositions of chondrite, primitive mantle, OIB, and N-MORB are from Sun and McDonough (1989). LCC is from Rudnick and Gao (2003).

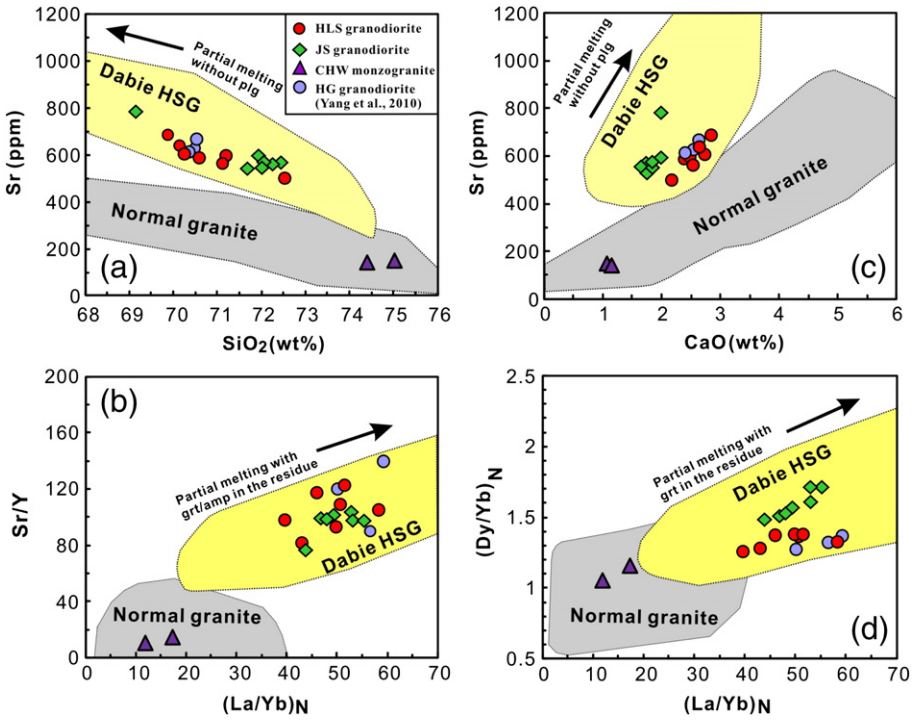

Fig. 7. Correlations between selected trace elements for Mesozoic granitoids from the Bengbu area. HLS (Huanglishan), Jingshan (JS), Huaiguang (HG), Changhuaiwei (CHW). Data of Huaiguang granodiorites are from Yang et al. (2010). The fields of high Sr/Y granitoids (HSG) and normal granites are from He et al. (2011). See text for the details.

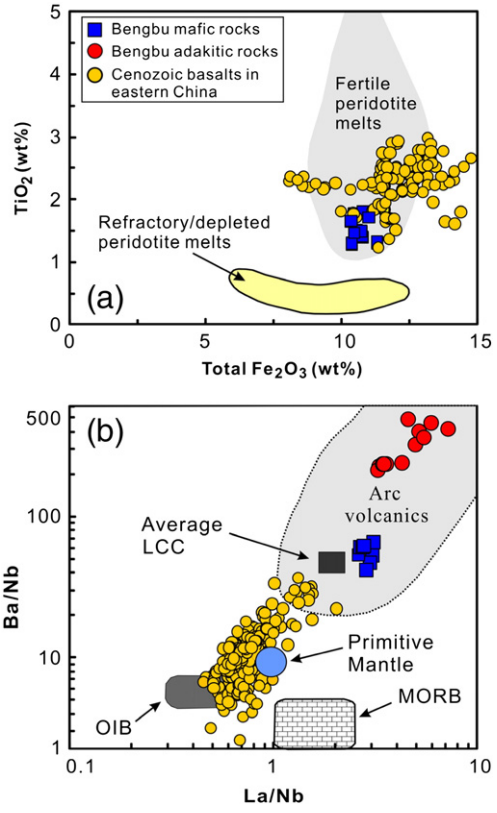

Fig. 8. (a) TiO_2 vs. total Fe_2O_3 plot for the Bengbu mafic rocks. The fields for peridotite melts were based on experiment results (Falloon et al., 1988). (b) Ba/Nb vs. La/Nb plot showing high Ba/Nb and La/Nb ratios of the Bengbu mafic rocks relative to the OIB and the primitive mantle. Cenozoic basalts from eastern China (Chen et al., 2007; Ho et al., 2003; Tang et al., 2006; Xu et al., 2005b; Zou et al., 2000) are also plotted for comparison. The fields for arc volcanics, MORB, OIB, and the primitive mantle after Jahn et al. (1999), and for average LCC after Rudnick and Gao (2003).

example, their Sr/Y and $(Dy/Yb)_N$ are positively correlated with $(La/Yb)_N$ (Fig. 7b, d) reflecting various extents of partial melting of eclogitic rocks in the presence of garnet. The lacking of Eu anomalies (Fig. 6b) and high Sr contents for a given SiO_2 or CaO (Fig. 7a, c), on the other hand, imply that plagioclase was little present in the mineral residues. In addition, their high K_2O/Na_2O (0.8–1.1) compared with oceanic adakites (generally<0.5) imply neglected amounts of amphiboles in the melting residue, indicating that their source was more likely thickened LCC other than subducted oceanic crust (Liu et al., 2010), since amphibole has much higher K_2O relative to garnet and clinopyroxene in the residues of metabasaltic melting (Rapp and Watson, 1995; Sen and Dunn, 1994). Hence, the melting residues during formation of the Bengbu granodiorites were most likely dominated by eclogite-facies mineral assemblage (garnet + cpx ± rutile), which would be denser than the mafic precursors as a result of garnets left behind during partial melting.

The distinct chemical features of the Bengbu granodiorites do not occur in the younger monzogranites. Compared to the granodiorites, the Bengbu monzogranites have much lower Sr, higher Y contents, and lower Sr/Y, La/Yb and $(Dy/Yb)_N$ values (Fig. 7), as well as prominent negative Eu anomalies (Fig. 6). These features indicate that the monzogranites have a shallower crustal provenance with plagioclase and without garnet in the residues. The low εHf (t) values of magmatic zircons and two-stage Hf model ages (T_{DM2}; 2.3–2.5 Ga) (Fig. 11b) further illustrate that the magma source region was in the ancient crust of the NCC for the Bengbu monzogranites.

5.2.2. Source attribute of the Bengbu granodiorites

The Sr–Nd–Pb isotopic signatures of the Bengbu granodiorites imply that their magma source was in an ancient LCC. The homogeneous, mantle-like oxygen isotopic compositions further support a LCC source without significant involvement of recycled surface materials. However, whether the ancient LCC source is from the NCC or the subducted SCB needs to be evaluated because crustal materials of the SCB had been subducted to the Bengbu area at or before Late Jurassic (Xu et al., 2005a). Elucidating the source nature of the granodiorites

Table 3
Whole-rock Sr–Nd–Pb isotopic compositions of granitoid and mafic dykes from the Bengbu area.

Sample	Rb ppm	Sr ppm	$^{87}Rb/^{86}Sr$	$^{87}Sr/^{86}Sr$	$^{87}Sr/^{86}Sr_i$	Sm ppm	Nd ppm	$^{147}Sm/^{144}Nd$	$^{143}Nd/^{144}Nd$	εNd (t)	$^{206}Pb/^{204}Pb$	$^{207}Pb/^{204}Pb$	$^{208}Pb/^{204}Pb$	$^{206}Pb/^{204}Pb$ (t)	$^{207}Pb/^{204}Pb$ (t)	$^{208}Pb/^{204}Pb$ (t)
Jingshan granodiorites																
JS-3	113.9	544	0.6054	0.71002	0.70903	2.71	17.86	0.0918	0.51157	−19.37	–	–	–	–	–	–
JS-4	109.5	580	0.5465	0.71014	0.70925	2.25	14.52	0.0938	0.51161	−18.46	17.087	15.441	37.631	17.017	15.438	37.569
JS-5	110.1	581	0.5486	0.71015	0.70926	2.15	13.6	0.0957	0.51161	−18.48	17.078	15.442	37.629	17.015	15.438	37.57
Huanglishan granodiorites																
HLS-01	90.65	592	0.4435	0.70891	0.70818	1.89	13.14	0.0869	0.51146	−21.29	16.644	15.365	37.207	16.589	15.363	37.156
HLS-02	85.48	591	0.4188	0.70892	0.70823	1.92	13.43	0.0867	0.51146	−21.42	16.660	15.376	37.246	16.609	15.374	37.189
HLS-1	61.26	349	0.5085	0.7089	0.70807	2.22	15.3	0.0878	0.51144	−21.70	16.569	15.334	37.132	16.524	15.331	37.047
HLS-3	75.87	460	0.4771	0.70867	0.70789	2.48	18.85	0.0796	0.51143	−21.81	16.598	15.341	37.121	16.565	15.339	37.063
HLS-9	101.6	425	0.6916	0.70865	0.70752	2.07	14.7	0.0851	0.51156	−19.43	16.671	15.356	37.118	16.636	15.354	37.064
Bengbu mafic dykes																
04JS-d1	95.35	867	0.3183	0.70692	0.70641	9.18	52.55	0.1056	0.51227	−5.96	17.262	15.406	37.68	16.999	15.393	37.257
04JS-d2	58.24	944	0.1785	0.70845	0.70816	10.3	58.20	0.1065	0.51227	−5.83	17.527	15.421	38.165	17.262	15.408	37.738
04JS-d3	9.82	629	0.04516	0.70665	0.70658	8.00	46.68	0.1036	0.51226	−6.03	17.420	15.431	38.101	17.155	15.419	37.675
JS-d1	14.19	420	0.0977	0.70701	0.70685	7.71	45.46	0.1026	0.51227	−5.87	17.419	15.44	38.085	17.154	15.427	37.659
JS-d2	11.16	429	0.07529	0.70695	0.70683	7.83	44.63	0.1061	0.51227	−5.89	17.231	15.426	37.861	16.967	15.413	37.438
JS-d6	11.42	547	0.06043	0.70665	0.70656	7.96	46.80	0.1029	0.51227	−5.84	17.044	15.399	37.618	16.782	15.386	37.197
JS-d7	12.48	573	0.06299	0.70679	0.70669	8.30	48.78	0.1029	0.51226	−5.96	17.462	15.442	38.102	17.196	15.429	37.676
JS-d8	37.57	896	0.1213	0.70734	0.70714	9.40	53.16	0.1069	0.51226	−6.07	17.323	15.397	37.872	17.059	15.384	37.448
HLS-d3	10.39	580	0.0518	0.70674	0.70666	7.31	43.02	0.1028	0.51227	−5.90	17.431	15.437	38.071	17.166	15.424	37.645

Notes: The internal analytical uncertainties (2σ) for $^{143}Nd/^{144}Nd$ and $^{87}Sr/^{86}Sr$ ratios are better than 0.00002, and for Pb isotopic ratios are better than 0.002 (2σ), which are not shown here especially for each sample. Initial isotopic ratios are calculated back to 112 Ma.

can also help to understand the deep crustal architecture of the Bengbu uplift.

Our zircon U–Pb dating results do not show any Neoproterozoic and Triassic ages in the Bengbu granodiorites, inconsistent with a source from subducted crust of the SCB; instead, the predominately Late Archean to Paleoproterozoic ages of inherited zircons agrees with the major growth periods of the NCC (Guo and Li, 2009b; Liu et al., 2009b; Zhao et al., 2001). Additionally, initial Sr–Nd–Pb isotopic compositions of the Bengbu granodiorites are similar to those of Early Cretaceous adakitic rocks from west Shandong in the NCC derived from partial melting of the mafic LCC of the NCC (Liu et al., 2009a), and also to those of Tushan amphibolite from Archean Wuhe Group (Figs. 9 and 10); but they are distinct from Mesozoic granitoids

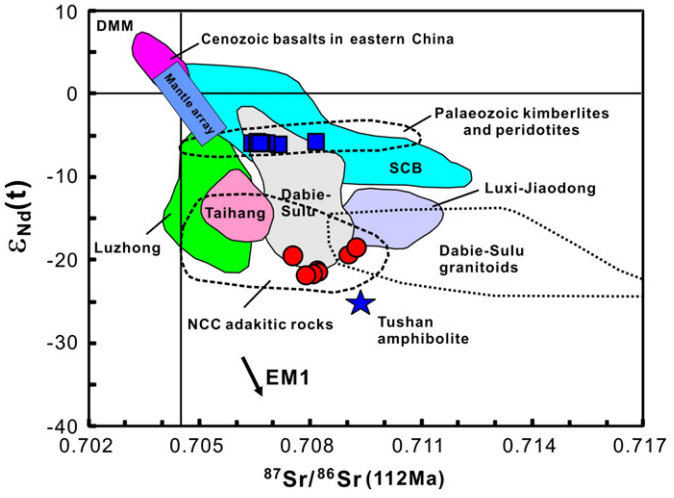

Fig. 9. Initial Sr and Nd isotopic correlation diagram of Mesozoic granitoids and mafic rocks from the Bengbu area. The fields for Mesozoic mafic rocks from other regions in the NCC (Luzhong, Taihang, Luxi-Jiaodong) and the South China Block (SCB) are after Huang et al. (2007b), for Palaeozoic kimberlites and peridotites are after Zheng and Lu (1999), and for Cenozoic basalts are as same as in Fig. 8. The fields for Mesozoic adakitic rocks from the NCC and Mesozoic granitoids from the Dabie–Sulu orogen are from He (2011). The data for Tushan amphibolite (blue star) which represents exposed LCC basement in the Bengbu area are our unpublished results. Note that the Bengbu mafic rocks have Sr–Nd isotopic compositions different from Mesozoic mafic rocks from any other regions in the NCC, and fall between the depleted mantle and the Bengbu low-Mg adakitic rocks or the Tushan amphibolite.

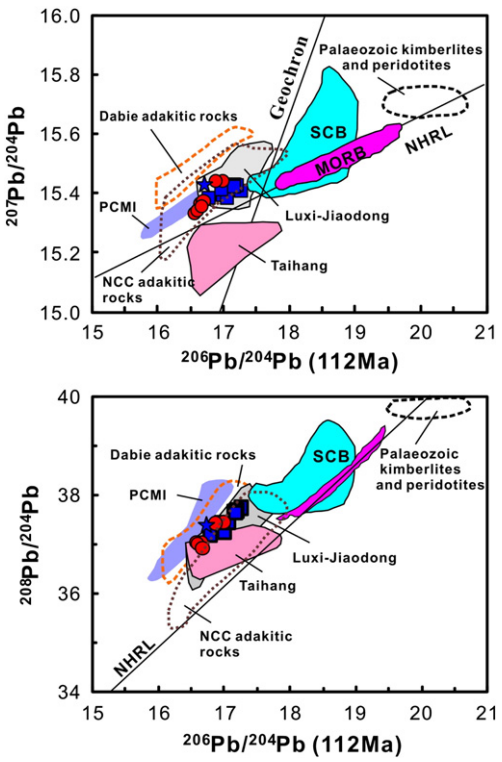

Fig. 10. Pb isotopic diagram of Mesozoic granitoids and mafic rocks from the Bengbu area. The data sources are as same as in Fig. 9. The post-collisional mafic intrusions (PCMI) from the Dabie Orogen (Huang et al., 2007a) are also plotted for comparison. The data for Tushan amphibolite (blue star) representing exposed LCC basement in the Bengbu area are our unpublished results. It is noted that Pb isotopic ratios of the Bengbu low-Mg adakitic rocks are similar to those of the NCC adakitic rocks but different from Dabie adakitic rocks, and $^{208}Pb/^{204}Pb$ ratios of the Bengbu mafic rocks are distinct from Dabie PCMI and fall between the depleted mantle and the Bengbu low-Mg adakitic rocks.

Table 4
In-situ zircon Hf and O isotopic compositions of granitoid rocks from the Bengbu area.

Age (Ma)	$^{176}Yb/^{177}Hf$	$^{176}Lu/^{177}Hf$	$^{176}Hf/^{177}Hf$	±2σ	$\varepsilon_{Hf}(t)$	±2σ	T_{DM1} (Ga)	T_{DM2} (Ga)	$\delta^{18}O$	2 se
Huanglishan granodiorite										
115.4	0.024302	0.000966	0.282163	0.000015	−19.0	0.3	1.54	2.37	5.84	0.22
1695	0.039587	0.001311	0.281591	0.000012	−4.9	0.2	2.35	2.71	6.51	0.30
2360	0.008116	0.000303	0.281347	0.000014	+1.0	0.3	2.61	2.80	5.94	0.27
115.0	0.018670	0.000726	0.282359	0.000013	−12.0	0.2	1.25	1.94	5.39	0.23
2035	0.035910	0.001382	0.282214	0.000015	−17.2	0.3	1.48	2.26	5.22	0.28
115.3	0.058366	0.002456	0.282257	0.000014	−16.0	0.2	1.46	2.18	5.53	0.24
115.8	0.030830	0.001169	0.282143	0.000014	−19.9	0.2	1.57	2.42	5.61	0.35
117.6	0.034626	0.001294	0.282185	0.000014	−18.5	0.2	1.52	2.33	5.86	0.38
2238	0.020228	0.000765	0.281324	0.000013	−2.3	0.2	2.68	2.94	6.07	0.30
115.4	0.002734	0.000106	0.282232	0.000012	−16.5	0.2	1.41	2.22	4.91	0.18
116.1	0.026991	0.001031	0.282096	0.000014	−21.3	0.3	1.63	2.52	6.24	0.20
114.6	0.034969	0.001386	0.282203	0.000019	−17.6	0.3	1.50	2.29	6.39	0.32
115.1	0.032352	0.001212	0.282178	0.000014	−18.7	0.3	1.52	2.35	5.89	0.26
116.9	0.031807	0.001210	0.282148	0.000011	−19.7	0.2	1.57	2.41	5.29	0.29
113.3	0.035812	0.001379	0.282239	0.000013	−16.5	0.2	1.44	2.21	6.32	0.28
111.3	0.002475	0.000098	0.282214	0.000014	−17.4	0.2	1.43	2.26	5.92	0.21
109.3	0.037108	0.001371	0.282426	0.000019	−10.0	0.3	1.18	1.80	6.18	0.33
2629	0.004374	0.000171	0.281310	0.000013	+7.0	0.2	2.65	2.67	6.39	0.34
Jingshan granodiorite										
120.9									5.42	0.30
119.5									5.62	0.27
128.5									5.90	0.39
119.8									5.63	0.22
118.2									5.10	0.28
119.9									5.32	0.29
116.5									5.31	0.42
Changhuaiwei granite										
113.6	0.032189	0.001242	0.282104	0.000013	−21.4	0.2	1.63	2.51	5.77	0.24
113.0	0.034730	0.001280	0.282165	0.000020	−19.1	0.4	1.55	2.38	5.84	0.26
109.1	0.031962	0.001186	0.282238	0.000017	−16.6	0.3	1.44	2.22	5.89	0.33
111.4	0.029452	0.001089	0.282127	0.000018	−20.6	0.3	1.59	2.46	5.73	0.31
97.5	0.032461	0.001218	0.282212	0.000016	−17.2	0.3	1.48	2.26	5.48	0.28
110.4	0.029741	0.001110	0.282058	0.000013	−22.4	0.2	1.69	2.60	5.12	0.29
113.4	0.020018	0.000770	0.282075	0.000015	−22.2	0.3	1.65	2.57	6.18	0.23
115.3	0.035379	0.001288	0.282187	0.000016	−18.4	0.3	1.51	2.33	6.12	0.29
112.0	0.033304	0.001267	0.282139	0.000015	−19.9	0.3	1.58	2.43	5.89	0.45
112.4	0.027077	0.001011	0.282217	0.000015	−17.1	0.3	1.46	2.25	5.73	0.32

Note that the ages of >1000 Ma quote $^{207}Pb/^{235}U$ ages and those of <1000 Ma are the $^{206}Pb/^{238}U$ ages.

from the Dabie Orogen in having lower $^{207}Pb/^{204}Pb$ at given $^{206}Pb/^{204}Pb$ (Fig. 10). Furthermore, two-stage Hf model ages (1.8–2.1 Ga) of the Bengbu granodiorites overlap with ages (1.8–1.9 Ga) of the Bengbu high-pressure granulites (Guo and Li, 2009b; Liu et al., 2009b). Overall, these lines of evidence suggest that the Bengbu granodiorites were directly derived from partial melting of the thickened mafic lower crust of the NCC, without reaction with the mantle as suggested by their low Mg# (<48).

5.3. Origin of mafic dykes in the Bengbu area

Late Mesozoic mafic igneous rocks throughout the eastern part of the NCC (such as Liaoxi, Taihang, Luzhong, Luxi, and Jiaodong) have been extensively investigated in previous studies (Guo et al., 2001; Xu et al., 2004; Yang and Li, 2008; Zhang et al., 2002, 2004). These rocks commonly show enriched Sr–Nd isotopic compositions (Figs. 9 and 10) and are genetically attributed to partial melting of the mantle sources hybridized by recycled continental crust. Some authors suggest that the recycled materials were the subducted crust of the SCB (Zhang et al., 2002, 2004), while others argue that the subcontinental lithospheric mantle was hybridized by foundering LCC of the NCC during the course of lithospheric thinning (Huang et al., 2007b; Liu et al., 2008; Yang and Li, 2008). In this study, for the first time, we report late Mesozoic mafic igneous rocks from the Bengbu area on south-eastern margin of the NCC (Fig. 1a), extending our understanding for the influence of recycled continental crust on the upper mantle beneath the NCC in the Mesozoic.

The Bengbu diabases have relatively high TiO_2 contents and plot in the field of experimental partial melts of fertile peridotites (Fig. 8a), comparable to Cenozoic basalts from eastern China that were primarily derived from an isotopically "depleted" mantle source. This implies derivation of the Bengbu diabases from the fertile asthenospheric mantle rather than the ancient, refractory sub-continental lithospheric mantle. This conclusion is reinforced by their different Pb isotopic compositions from Paleozoic kimberlites in the NCC as discussed below. However, their strongly enriched LREE relative to HREE, distinct depletion of Nb, Ta, Zr, Hf and Ti, positive Pb anomalies and high K contents (Fig. 6c) suggest that the mantle source regions contained a significant contribution from components of the continental crust or subducted oceanic crust. This is consistent with their lower Nb/U, higher La/Nb and Ba/Nb ratios relative to the primitive mantle as well as Cenozoic basalts from eastern China (Fig. 8b).

The Sr–Nd–Pb isotopic data provide direct constraints on nature of the recycling crustal materials. The lacking of correlations of $^{87}Sr/^{86}Sr_i$ and εNd (t) with MgO contents of the Bengbu diabases, e.g., uniform εNd (t) values over the overall range of MgO, suggest that crustal contamination is insignificant. Although Sr and Nd isotopic compositions of the Bengbu diabases overlap with the Paleozoic kimberlites and their borne garnet peridotite xenoliths in the NCC (Fig. 9) which sampled the Paleozoic lithospheric mantle (Zheng and Lu, 1999), they are dramatically distinct in Pb isotopic compositions (Fig. 10). This suggests that the ancient lithospheric mantle, as least beneath the Bengbu area, might have been removed and replaced with a newly accreted lithospheric mantle, i.e., the depleted upper mantle with

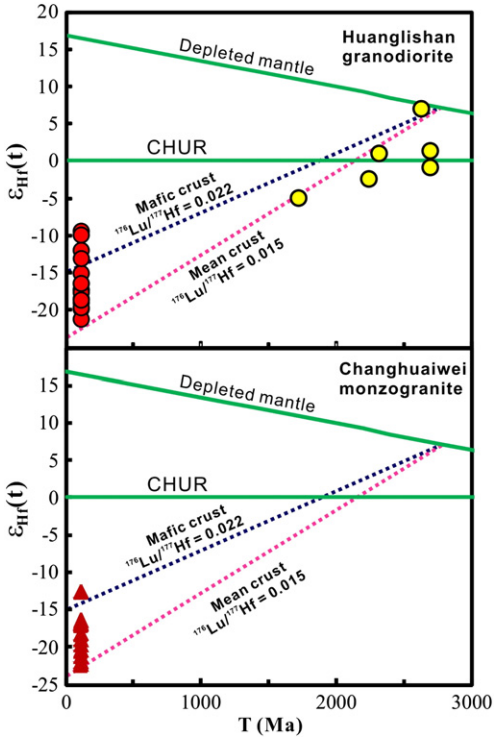

Fig. 11. Hf isotopic evolution of the Bengbu granodiorites (Huanglishan) and granites (Changhuaiwei). The yellow circle represents inherited zircon domains in the Huanglishan granodiorites. Data are reported in Supplementary Table 1.

involvement of recycling crust. In detail, the low radiogenic Pb of the Bengbu diabases (e.g., $^{206}Pb/^{204}Pb_i < 17.2$) argue against derivation of the recycling components from the subducted oceanic crust sediments or the upper continental crust which both have high radiogenic Pb (e.g., $^{206}Pb/^{204}Pb_i > 18.0$) (Plank and Langmuir, 1998). Instead, the ancient (Archean to Early Paleoproterozoic) LCC was the most likely candidate given their time-integrated unradiogenic Pb (e.g., Bolhar et al., 2007). Interestingly, $^{207}Pb/^{204}Pb$ and $^{206}Pb/^{204}Pb$ ratios of the Bengbu diabases fall between the depleted MORB mantle (DMM) end-member and the regional LCC sampled by the Bengbu low-Mg adakitic rocks and the exposed Archean LCC rocks in the Bengbu area (Fig. 10), suggesting that the mantle source likely contained the recycled ancient LCC. As discussed earlier, the crustal materials of the subducted SCB might have reached underneath the Bengbu area at or before the late Jurassic. Thus whether the subducted SCB crust had also contributed to the genesis of the Bengbu diabases should be assessed. For a given $^{206}Pb/^{204}Pb$, the $^{208}Pb/^{204}Pb$ ratios (or $\Delta 8/4$ values) of the Bengbu diabases are lower than those of the Late Mesozoic post-collision mafic intrusions (PCMI) from the Dabie Orogen (Fig. 10), which originated from the mantle source hybridized by recycled SCB lower crust (Huang et al., 2007a). This precludes the affiliation of the Late Mesozoic lithospheric mantle beneath the Bengbu area is similar to the subducted continental crust of the SCB. Initial Sr–Nd isotopic data of the Bengbu diabases also fall between the DMM and the Bengbu low-Mg adakitic rocks or the exposed LCC rocks (Fig. 9), further suggesting their derivation from the depleted mantle that was subject to modification by the infiltration of melts from recycled lower crust of the NCC.

To evaluate the above conclusion, we modeled the two-members mixing process and plot the results in Fig. 12. The modeling results show that adding approximately 10–15% of the regional LCC to the depleted mantle could consistently interpret the isotopic and trace elemental characteristics observed in the Bengbu diabases (Fig. 12). In addition, involvement of the LCC materials could also readily account for other features of the Bengbu diabases such as LREE enrichment and HFSE (Nb, Ta, Ti) depletion as well as positive anomalies of Pb.

5.4. Implications for lithospheric thinning of the NCC

Two prevailing models have been proposed for Mesozoic lithospheric thinning of the NCC: prolonged "bottom-up" thermo-chemical erosion (Menzies et al., 2007; Xu, 2001; Xu et al., 2004), and rapid "down-up" delamination/foundering from the over-thickened LCC (Gao et al., 2004; Ling et al., 2009; Liu et al., 2009a; Xu et al., 2006b; Yang et al., 2005). The overall ~100 Ma (from Early Jurassic to late Cretaceous) duration of Mesozoic magmatism throughout the entire NCC has been used to argue for the thermo-chemical model. However, the Mesozoic magmatism in the NCC was usually discrete, comprising multiple episodes including Triassic, Jurassic and Cretaceous (e.g., Yang et al., 2008). In addition, in many regions particularly in the interior of the craton (e.g. Taihang and Luxi), the Early Jurassic magmatism was largely missing and there was a clear magmatism peak at the Early Cretaceous (Chen et al., 2008; Wu et al., 2005a). This is also the case in the Bengbu area (this study; Yang et al., 2010). Therefore, lithospheric thinning may be considered to be spatially and temporally heterogeneous throughout the NCC, and it probably took place mainly at a considerably short timescale in some regions.

In the early stages of lithospheric thinning, thermal–chemical erosion due to convection of deep (hot) asthenosphere might have played an important role in reactivating the lithospheric keel, elevating the geothermal gradient of lithosphere and resulting in melting of the crust to generate large amounts of granitic plutons. But it alone is difficult to explain (1) the generation of high-Mg adakitic lavas/intrusions which requires recycling of the dense LCC into the mantle from the overlying crust (Gao et al., 2004; Liu et al., 2009a; Xu et al., 2006b), (2) the presence of lower crustal components in mantle source region of Mesozoic basaltic igneous rocks in the NCC (Huang et al., 2007b; Ling et al., 2009; Liu et al., 2008; Yang and Li, 2008), and (3) a clear peak of Mesozoic magmatism throughout the NCC (Wu et al., 2005a). Although the delamination model appears to match with these above observations, it requires a trigger mechanism for causing enough gravitational instability and weakening of the lithosphere, a key factor for lithospheric foundering that has not been well constrained yet. Recently He et al. (2011) proposed that partial

Table 5
Summary of age data of Early Cretaceous igneous rocks in the Bengbu area.

Pluton	Rock type	Comments	Age (Ma)	Inherited zircons	Method	Source
Jingshan	Granodiorite	Adakitic	118 ± 1	1.87 Ga	SIMS	This study
Jingshan	porphyry granodiorite	Adakitic	123 ± 4	1.87 Ga	SHRIMP	This study
Huanglishan	Granodiorite	Adakitic	115 ± 1	1.56–2.63 Ga	SIMS	This study
			118 ± 3	1.70–2.73 Ga	LA-ICP-MS	This study
Huaiguang	Granodiorite	Adakitic	130 ± 2	1.81–3.44 Ga	SHRIMP	Yang et al., 2010
Changhuaiwei	Monzogranite	Normal	112 ± 1	–	SIMS	This study
Caoshan	Monzogranite	Normal	112 ± 2	–	LA-ICP-MS	Yang et al., 2010
Jingshan	Diabase	Mafic	111.8 ± 0.6	–	Ar–Ar	This study
Xilushan	Seynogranite	"Indefinite"	129 ± 5	168–528 Ma	LA-ICP-MS	Yang et al., 2010

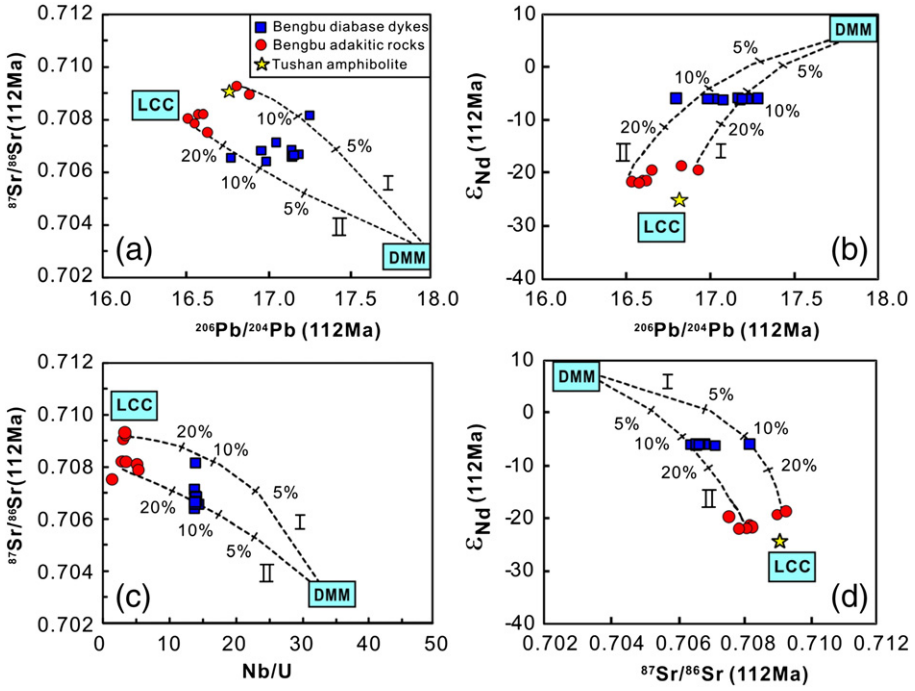

Fig. 12. Modeling results for mixing between the depleted MORB mantle (DMM) and the regional lower crust in the Bengbu area as sampled by the low-Mg adakitic rocks. The Bengbu mafic rocks could be produced by partial melting of the depleted mantle with 10–15% regional lower crust. The parameters for DMM are assumed the following: $^{87}Sr/^{86}Sr = 0.703$, $^{143}Nd/^{144}Nd = 0.51307$ or $\varepsilon_{Nd} = +8.5$, $^{206}Pb/^{204}Pb = 18$; Sr = 20 ppm, Nd = 1.2 ppm, Pb = 0.2 ppm.
The Sr, Nd, Pb, Nb and U contents of the lower crust from Rudnick and Gao (2003).

melting of the pre-existing thickened LCC and segregation of widespread felsic melts from the LCC may serve as the major trigger for lithospheric foundering in the Dabie collisional orogen. This case study in Bengbu area suggests a similar trigger mechanism for lithospheric foundering on the south-eastern margin of the NCC.

The identification of adakitic rocks in the Bengbu area suggests that there was a thickened (~45 km and perhaps extending 50 km) LCC on south-eastern margin of the NCC in the Early Cretaceous, and the thickened LCC had not been removed before emplacement of the adakitic granodiorites at 130–115 Ma. Previous studies of eclogitic xenoliths entrained in Early Cretaceous high-Mg# diorites from the Xu-Huai area (~100 km north of Bengbu) also suggest that the crust thickness exceeded ~50 km (>1.5 GPa) on south-eastern margin of the NCC, probably due to continent–continent collision between the NCC and the SCB (Xu et al., 2006a). The nowadays crust in the eastern NCC (e.g., Shandong) is, however, estimated to be ca. 32 km thickness based on gravity and magnetism (Jiang et al., 2000) indicating that the Mesozoic thickened LCC were considerably thinned at some time between Mesozoic and present day. Since no adakitic signature in granitic rocks in the Bengbu area has been observed since ~112 Ma, a preferred hypothesis is such that the thickened LCC was rapidly removed between 115 and 112 Ma. This hypothesis could plausibly explain the change of crustal thickness on the basis of contrasting chemistry of adakitic rocks and granites, and the genetic association between adakitic rocks and mafic dykes. We described explicitly the two-stage model below.

At the first stage, the pre-existing thickened LCC underwent partial melting at 130–115 Ma, generating the low-Mg# adakitic granodiorites. Partial melting of the thickened LCC left behind denser residues as a result of extraction of felsic adakitic melts, and the residues became increasedly dense as partial melting proceeded and melt generation increased. Experimental studies show that melting of tonalitic compositions at pressures of >20 kbar with generation of a moderate amount (20–30%) of melts leaves the residues having densities of ≥3.3 g/cm^3 (Patino Douce, 2005), thus melting of mafic precursors at similar extents of melt extraction was expected to yield residues denser than mantle rocks (3.3 g/cm^3). In addition, the viscosity of the thickened LCC would be remarkably decreased by melting of the LCC itself due to generation of partial melts. Consequently, gravitational instability of the residual LCC and its weakening enhanced by partial melting enabled detachment of this LCC layer from the overlying remaining crust. The detached dense LCC layer, in conjunction with the underlying lithospheric mantle, could then sink into the asthenospheric mantle between 115 and 112 Ma. Note that in this first stage there might also be concomitant generation of little amount of normal granitic rocks together with adakitic rocks, due to melting of the middle–lower crust similar to that observed in the Dabie Orogen (He et al., 2011). However, we highlight here that no adakitic rocks were produced after this stage.

At the second stage, the foundered LCC was mixed with the upwelling, hot asthenospheric mantle forming a hybridized mantle source. This newly formed, hybridized mantle replaced the volume formerly occupied by the foundered lithosphere, resulting in "continental" geochemical signatures observed in the mafic dykes. Meanwhile, influx of heat sources from upwelling mantle induced widespread partial melting of the thinned crust, generating normal granitic rocks (e.g., Bengbu monzogranites) that do not have chemical characteristics of adakites due to low pressures of partial melting.

Notably, the characteristic magma sequence observed here was not exclusive on the south margin in the NCC. For example, on the north margin of the NCC (e.g., Liaodong), the Jurassic magmatism was also dominated by granitoids with the majority showing adakitic characteristics and the mafic rocks (veins) were formed subsequent to granitoids at the Early Cretaceous (Wu et al., 2005b). Furthermore, the temporal sequence of Mesozoic magmatism in the Bengbu area is also quite similar to that found in the Dabie Orogen in central China, where normal (non-adakitic) granites and mafic intrusions or lavas (<130 Ma) were formed generally later than the low-Mg adakitic granitoid rocks (143–130 Ma). The temporal difference of various types of magmatism in turn indicates that the over-thickened mountain root underneath the Dabie Orogen, which formed during Triassic continent–continent collision, was removed at around 130 Ma (He et

al., 2011). Collectively, these observations suggest a similar kinetic mechanism and process for lithospheric thinning/removal in the studied area and the Dabie Orogen, and this proposed model may be of universal significance for foundering and recycling of the LCC in orogenic belts and cartonic margins, where the crust underwent pre-thickening by continent–continent collisions and the thickened lithosphere had kept gravitationally stable over a long timescale.

In this two-stage model of lithospheric thinning, an important issue is what was the principal heat source required for the initial melting of crustal rocks starting at ~130–115 Ma on the south-eastern margin of the NCC. This could not be directly linked to Triassic subduction of the SCB and its subsequent collision with the NCC because of the long temporal interval (~100 Ma). Recently, increasing studies suggest that Mesozoic–Cenozoic subduction of the Pacific plate played an important role in activation and destruction of the NCC lithosphere (e.g., Sun et al., 2007; Zhao et al., 2007; Zhang et al., 2009; Zhu and Zheng, 2009). The subduction process might induce mantle flow and melting of the lithosphere in the eastern NCC, but a clear role has not been evidenced in the studied area. Alternatively, it is noted that Mesozoic magmatism in the Bengbu area was formed significantly later than that in the Dabie orogen. As mentioned above, the mountain root removal underneath the Dabie Orogen and the mantle upwelling occurred at around 130 Ma, which coincides with the time of initial melting of the thickened continental crust in the Bengbu area. This suggests that re-activation of the lithosphere on the southeastern margin of the NCC was possibly induced by the early Cretaceous mantle upwelling caused by mountain-root collapse of the adjacent Dabie Orogen on the south. In this case, the mountain-root removal of the circle-craton orogens could play an important role in decratonization of the cratonic margins.

6. Conclusion

Mesozoic granitoids and mafic rocks from the Bengbu area on the south-eastern margin of the NCC provide an opportunity to understand the mechanism and processes of lithospheric thinning in the North China Craton. Precise geochronological results along with field-based observations show that the granodiorites in the Bengbu area were formed at 123–115 Ma, prior to the granites and mafic dykes (both at ~112 Ma). The granodiorites are geochemically similar to high-SiO_2 (or low-Mg#) adakites and were derived from partial melting of the thickened LCC of the NCC. In contrast, the granites show lacking of adakitic characteristics and were originated from the shallower crust. The mafic rocks were derived from partial melting of the upwelling upper mantle hybridized by the foundered LCC of the NCC.

We proposed a hypothesis that partial melting of the pre-existing thickened LCC weakened the LCC and left behind a dense (eclogite) residue as a result of felsic melt extraction, which could founder into the mantle due to negative buoyancy. The proposed two-stage model of lithospheric thinning could reasonably explain the genesis of these various types of igneous rocks and their characteristic formation sequence. Such a process of lithospheric thinning is similar to the post-collisional mountain-root collapse in the Dabie Orogen of central China, suggesting that this model has broad significance for foundering of a thickened lower crust in settings of orogenic belts and cratonic margins.

Acknowledgment

We are grateful to Yican Liu, Yilin Xiao, Shuijiong Wang, Xianjun Dai for their help during field work. Thanks are due to Chaofeng Li, Jinrong Li, Shizhen Li, Xianhua Li, Qiuli Li and Yu Liu for assistance with element analysis, Sr, Nd and Pb isotope measurement and zircon U–Pb dating. Drs. Fang Huang, Jingao Liu, Wei Yang and Fangzhen Teng are acknowledged for stimulating discussion. We thank the reviewers for constructive comments and Nelson Eby for efficient editing that helped improve the presentation. This work is supported by the National Natural Foundation of China (40634023, 90814008, 40921002, and 91014007).

Appendix A. Supplementary data

Supplementary data to this article can be found online at doi:10.1016/j.lithos.2011.12.015.

References

Black, L.P., Kamo, S.L., Allen, C.M., Davis, D.W., Aleinikoff, J.N., Valley, J.W., Mundil, R., Campbell, I.H., Korsch, R.J., Williams, I.S., Foudoulis, C., 2004. Improved $^{206}Pb/^{238}U$ microprobe geochronology by the monitoring of a trace-element-related matrix effect; SHRIMP, ID-TIMS, ELA-ICP-MS and oxygen isotope documentation for a series of zircon standards. Chemical Geology 205, 115–140.

Bolhar, R., Kamber, B.S., Collerson, K.D., 2007. U–Th–Pb fractionation in Archaean lower continental crust: implications for terrestrial Pb isotope systematics. Earth and Planetary Science Letters 254, 127–145.

Castillo, P.R., Janney, P.E., Solidum, R.U., 1999. Petrology and geochemistry of Camiguin Island, southern Philippines: insights to the source of adakites and other lavas in a complex arc setting. Contributions to Mineralogy and Petrology 134, 33–51.

Chen, B., Jahn, B.M., Zhai, M.G., 2004. Petrogenesis of the Mesozoic intrusive complexes from the southern Taihang Orogen, North China Craton: element and Sr–Nd–Pb isotopic constraints. Contributions to Mineralogy and Petrology 148, 489–501.

Chen, Y., Zhang, Y., Graham, D., Su, S., Deng, J., 2007. Geochemistry of Cenozoic basalts and mantle xenoliths in Northeast China. Lithos 96, 108–126.

Chen, B., Tian, W., Jahn, B.M., Chen, Z.C., 2008. Zircon SHRIMP U–Pb ages and in-situ Hf isotopic analysis for the Mesozoic intrusions in South Taihang, North China craton: evidence for hybridization between mantle-derived magmas and crustal components. Lithos 102, 118–137.

Defant, M., Drummond, M., 1990. Derivation of some modern arc magmas by melting of young subducted lithosphere. Nature 347, 662–665.

Falloon, T.J., Green, D.H., Hatton, C.J., Harris, K.L., 1988. Anhydrous partial melting of a fertile and depleted peridotite from 2 to 30 kb and application to basalt petrogenesis. Journal of Petrology 29, 1257–1282.

Fan, W.M., Menzies, M.A., 1992. Destruction of aged lower lithosphere and accretion of asthenosphere mantle beneath eastern China. Geotectonica et Metallogenia 16, 171–180.

Fan, W.M., Zhang, H.F., Baker, J., Jarvis, K.E., Mason, P.R.D., Menzies, M.A., 2000. On and off the north China craton: where is the Archaean keel? Journal of Petrology 41, 933–950.

Gao, S., Rudnick, R.L., Yuan, H.-L., Liu, X.-M., Liu, Y.-S., Xu, W.-L., Ling, W.-L., Ayers, J., Wang, X.-C., Wang, Q.-H., 2004. Recycling lower continental crust in the North China craton. Nature 432, 892–897.

Griffin, W.L., Andi, Z., O'Reilley, S.Y., Ryan, C.G., 1998. Planerozoic evolution of the lithosphere beneath the Sino–Korean craton. Mantle dynamics and plate interactions in East Asia. American Geophysical Union, Geodynamics Series 27, 107–126.

Guo, S.-S., Li, S.G., 2009a. Petrochemical characteristics of leucogranite and a case study of Bengbu leucogranites. Chinese Science Bulletin 54, 1923–1930.

Guo, S.-S., Li, S.G., 2009b. Zircon SHRIMP U–Pb ages constrained the early Proterozoic events of metamorphism and magmatism on the south-eastern margin of the North China craton. Science in China Series D — Earth Sciences 39, 1039–1045.

Guo, F., Fan, W.M., Wang, Y.J., Lin, G., 2001. Late Mesozoic mafic intrusive complexes in North China Block: constraints on the nature of subcontinental lithospheric mantle. Physics and Chemistry of the Earth (A) 26, 759–771.

He, Y., 2011. Geochemistry of post-collisional granitic Magmatism from the Dabie orogen: Constraints on removal processes and architecture of the mountain root. A dissertation for doctor's degree. University of Science and Technology of China (in Chinese with English abstract).

He, Y., Li, S.G., Hoefs, J., Huang, F., Liu, S.-A., Hou, Z., 2011. Post-collisional granitoids from the Dabie orogen: new evidence for partial melting of a thickened continental crust. Geochimica et Cosmochimica Acta 75, 3815–3838.

Ho, K., Chen, J., Lo, C., Zhao, H., 2003. 40Ar/39Ar dating and geochemical characteristics of late Cenozoic basaltic rocks from the Zhejiang–Fujian region, SE China: eruption ages, magma evolution and petrogenesis. Chemical Geology 197, 287–318.

Huang, F., Li, S.G., Dong, F., Li, Q.L., Chen, F.K., Wang, Y., Yang, W., 2007a. Recycling of deeply subducted continental crust in the Dabie Mountain, central China. Lithos 96, 151–169.

Huang, F., Li, S.G., Yang, W., 2007b. Contributions of the lower crust to Mesozoic mantle-derived matic rocks from the North China Craton: implications for lithospheric thinning. Geological Society, London, Special Publications 280, 55–75.

Irvine, T.N., Babagar, W.R.A., 1971. A guide to the chemical classification of the common volcanic rocks. Can. J. Earth Sci. 8, 523–548.

Jahn, B.M., Wu, F.Y., Lo, C.H., Tsai, C.H., 1999. Crust–mantle interaction induced by deep subduction of the continental crust: geochemical and Sr–Nd isotopic evidence from post-collisional mafic–ultramafic intrusions of the northern Dabie complex, central China. Chemical Geology 157, 119–146.

Jiang, W.W., Hao, T.Y., Jiao, C.M., Song, H.B., 2000. The characters of gravity and magnetic field and crustal structure from Qingzhou to Muping, Shandong Province. Geophysics Processes 15, 18–26.

Kamei, A., Miyake, Y., Owada, M., Kimura, J.I., 2009. A pseudo adakite derived from partial melting of tonalitic to granodioritic crust, Kyushu, southwest Japan arc. Lithos 112, 615–625.
Klein, M., Stosch, H.G., Seck, H., Shimizu, N., 2000. Experimental partitioning of high field strength and rare earth elements between clinopyroxene and garnet in andesitic to tonalitic systems. Geochimica et Cosmochimica Acta 64, 99–115.
Li, S.G., Xiao, Y.L., Liou, D.L., Chen, Y.Z., Ge, N.J., Zhang, Z.Q., Sun, S.S., Cong, B.L., Zhang, R.Y., Hart, S.R., Wang, S.S., 1993. Collision of the North China and Yangtze Blocks and formation of coesite-bearing eclogites — timing and processes. Chemical Geology 109, 89–111.
Li, S.G., Jagoutz, E., Chen, Y.Z., Li, Q.L., 2000. Sm–Nd and Rb–Sr isotopic chronology and cooling history of ultrahigh pressure metamorphic rocks and their country rocks at Shuanghe in the Dabie Mountains, Central China. Geochimica et Cosmochimica Acta 64, 1077–1093.
Li, X.H., Li, W.X., Wang, X.C., Li, Q.L., Liu, Y., Tang, G.Q., 2009. Role of mantle-derived magma in genesis of early Yanshanian granites in the Nanling Range, South China: in situ zircon Hf–O isotopic constraints. Sci China Ser D — Earth Sci 39, 872–887.
Li, Q.-L., Li, X.-H., Liu, Y., Wu, F.-Y., Yang, J.-H., Mitchell, R.H., 2010. Precise U–Pb and Th–Pb age determination of kimberlitic perovskites by secondary ion mass spectrometry. Chemical Geology 269, 396–405.
Ling, W.-L., Duan, R.-C., Xie, X.-J., Zhang, Y.-Q., Zhang, J.-B., Cheng, J.-P., Liu, X.-M., Yang, H.-M., 2009. Contrasting geochemistry of the Cretaceous volcanic suites in Shandong province and its implications for the Mesozoic lower crust delamination in the eastern North China craton. Lithos 113, 640–658.
Liu, Y.S., Gao, S., Kelemen, P.B., Xu, W.L., 2008. Recycled crust controls contrasting source compositions of Mesozoic and Cenozoic basalts in the North China Craton. Geochimica et Cosmochimica Acta 72, 2349–2376.
Liu, S., Hu, R.Z., Gao, S., Feng, C.X., Yu, B.B., Qi, Y.Q., Wang, T., Feng, G.Y., Coulson, I.M., 2009a. Zircon U–Pb age, geochemistry and Sr–Nd–Pb isotopic compositions of adakitic volcanic rocks from Jiaodong, Shandong Province, Eastern China: constraints on petrogenesis and implications. Journal of Asian Earth Sciences 35, 445–458.
Liu, Y.C., Wang, A.D., Rolfo, F., Groppo, C., Gu, X.F., Song, B., 2009b. Geochronological and petrological constraints on Palaeoproterozoic granulite facies metamorphism in southeastern margin of the North China Craton. Journal of Metamorphic Geology 27, 125–138.
Liu, S.-A., Li, S.G., He, Y.S., Huang, F., 2010. Geochemical contrasts between early Cretaceous ore-bearing and ore-barren high-Mg adakites in central-eastern China: implications for petrogenesis and Cu–Au mineralization. Geochimica et Cosmochimica Acta 74, 7160–7178.
Ludwig, K.R., 2001. Users Manual for Isoplot/Ex (rev.2.4.9): A geochronological Toolkit for Microsoft Excel. Berkeley Geochronology Center. Special Publication, No.1a: 55 pp.
Macpherson, C.G., Dreher, S.T., Thirlwall, M.F., 2006. Adakites without slab melting: high pressure differentiation of island arc magma, Mindanao, the Philippines. Earth and Planetary Science Letters 243, 581–593.
Martin, H., Smithies, R.H., Rapp, R., Moyen, J.F., Champion, D., 2005. An overview of adakite, tonalite–trondhjemite–granodiorite (TTG), and sanukitoid: relationships and some implications for crustal evolution. Lithos 79, 1–24.
Menzies, M.A., Fan, W.M., Zhang, M., 1993. Paleozoic and Cenozoic lithoprobes and the loss of >120 km of Archean lithosphere, Sino–Korean Craton, China. Magmatic processes and plate tectonics. Geological Society Special Publication 76, 71–81.
Menzies, M.A., Xu, Y.G., Zhang, H.F., Fan, W.M., 2007. Integration of geology, geophysics and geochemistry: a key to understanding the North China Craton. Lithos 96, 1–21.
Moyen, J.F., 2009. High Sr/Y and La/Yb ratios: the meaning of the "adakitic signature". Lithos 112, 556–574.
Patino Douce, A.E., 2005. Vapor-absent melting of tonalite at 15–32 kbar. Journal of Petrology 46, 275–290.
Pertermann, M., Hirschmann, M., Hametner, K., Günther, D., Schmidt, M., 2004. Experimental determination of trace element partitioning between garnet and silica-rich liquid during anhydrous partial melting of MORB-like eclogite. Geochemistry Geophysics Geosystems 5, Q05A01.
Plank, T., Langmuir, C.H., 1998. The chemical composition of subducting sediment and its consequences for the crust and mantle. Chemical Geology 145, 325–394.
Qiu, R.L., Xu, X., Huang, D.Z., 1999. The isotopic age of the Jingshan intrusive in the Bengbu region of the southeastern edge of the North China block and its geological implications. Geology of Anhui (China) 9, 161–164.
Rapp, R.P., Watson, E.B., 1995. Dehydration melting of metabasalt at 8–32 kbar: implications for continental growth and crust–mantle recycling. Journal of Petrology 36, 891–931.
Rudnick, R.L., Gao, S., 2003. Composition of the continental crust. In The Crust (ed. R L Rudnick) Vol. 3 Treatise on Geochemistry (eds. H D Holland and K K Turekian), Elsevier-Pergamon, Oxford. pp. 1–64.
Sen, C., Dunn, T., 1994. Dehydration melting of a basaltic composition amphibolite at 1.5 and 2.0 GPa: implications for the origin of adakites. Contributions to Mineralogy & Petrology 117, 394–409.
Skjerlie, K.P., Johnston, A.D., 1996. Vapour-absent melting from 10 to 20 kbar of crustal rocks that contain multiple hydrous phases: implications for anatexis in the deep to very deep continental crust and active continental margins. Journal of Petrology 37, 661–691.
Sun, S., McDonough, W., 1989. Chemical and isotopic systematics of oceanic basalts: implications for mantle composition and processes. Geological Society London Special Publications 42, 313.
Sun, W., Ding, X., Hu, Y.H., Li, X.H., 2007. The golden transformation of the Cretaceous plate subduction in the west Pacific. Earth and Planetary Science Letters 262, 533–542.
Tang, Y.-J., Zhang, H.-F., Ying, J.-F., 2006. Asthenosphere–lithospheric mantle interaction in an extensional regime: implication from the geochemistry of Cenozoic basalts from Taihang Mountains, North China Craton. Chemical Geology 233, 309–327.
Wang, Q., Wyman, D.A., Xu, J.F., Jian, P., Zhao, Z.H., Li, C.F., Xu, W., Ma, J.L., He, B., 2007. Early Cretaceous adakitic granites in the Northern Dabie Complex, central China: implications for partial melting and delamination of thickened lower crust. Geochimica et Cosmochimica Acta 71, 2609–2636.
Wu, F.-Y., Lin, J.Q., Wilde, S.A., Zhang, X.O., Yang, J.-H., 2005a. Nature and significance of the Early Cretaceous giant igneous event in eastern China. Earth and Planetary Science Letters 233, 103–119.
Wu, F.-Y., Yang, J.-H., Wilde, S.A., Zhang, X.O., 2005b. Geochronology, petrogenesis and tectonic implications of the Jurassic granites in the Liaodong Peninsula, NE China. Chemical Geology 221, 127–156.
Xu, Y.G., 2001. Thermo-tectonic destruction of the Archean lithospheric keel beneath the Sino–Korean Craton in China: evidence, timing and mechanism. Physics and Chemistry of the Earth (A) 26, 747–757.
Xu, Y., Huang, X., Ma, J., Wang, Y., Iizuka, Y., Xu, J., Wang, Q., Wu, X., 2004. Crust–mantle interaction during the tectono-thermal reactivation of the North China Craton: constraints from SHRIMP zircon U˙CPb chronology and geochemistry of Mesozoic plutons from western Shandong. Contributions to Mineralogy and Petrology 147, 750–767.
Xu, W.L., Wang, Q.H., Yang, D.B., Liu, X.C., Guo, J.H., 2005a. SHRIMP zircon U–Pb dating in Jingshan "migmatitic granite", Bengbu and its geological significance. Science in China Series D — Earth Sciences 48, 185–191.
Xu, Y.-G., Ma, J.-L., Frey, F.A., Feigenson, M.D., Liu, J.-F., 2005b. Role of lithosphere–asthenosphere interaction in the genesis of Quaternary alkali and tholeiitic basalts from Datong, western North China Craton. Chemical Geology 224, 247–271.
Xu, W.L., Gao, S., Wang, Q.H., Wang, D.Y., Liu, Y.S., 2006a. Mesozoic crustal thickening of the eastern North China Craton: evidence from eclogite xenoliths and petrologic implications. Geology 34, 721–724.
Xu, W.L., Wang, Q.H., Wang, D.Y., Guo, J.H., Pei, F.P., 2006b. Mesozoic adakitic rocks from the Xuzhou–Suzhou area, eastern China: evidence for partial melting of delaminated lower continental crust. Journal of Asian Earth Sciences 27, 230–240.
Yang, W., Li, S.G., 2008. Geochronology and geochemistry of the Mesozoic volcanic rocks in Western Liaoning: implications for lithospheric thinning of the North China Craton. Lithos 102, 88–117.
Yang, J.H., Wu, F.Y., Chung, S.L., Wilde, S.A., Chu, M.F., Lo, C.H., Song, B., 2005. Petrogenesis of Early Cretaceous intrusions in the Sulu ultrahigh-pressure orogenic belt, east China and their relationship to lithospheric thinning. Chemical Geology 222, 200–231.
Yang, J.-H., Wu, F.-Y., Wilde, S.A., Belousova, E., Griffin, W.L., 2008. Mesozoic decratonization of the North China block. Geology 36, 467–470.
Yang, D.B., Xu, W.L., Wang, Q.H., Pei, F.P., 2010. Chronology and geochemistry of Mesozoic granitoids in the Bengbu area, central China: constraints on the tectonic evolution of the eastern North China Craton. Lithos 114, 200–216.
Zhang, H.F., Sun, M., Zhou, X.H., Fan, W.M., Zhai, M.G., Ying, J.F., 2002. Mesozoic lithosphere destruction beneath the North China Craton: evidence from major-, trace-element and Sr–Nd–Pb isotope studies of Fangcheng basalts. Contributions to Mineralogy and Petrology 144, 241–253.
Zhang, H.F., Sun, M., Zhou, M.F., Fan, W.M., 2004. Highly heterogeneous late Mesozoic lithospheric mantle beneath the North China craton: evidence from Sr–Nd–Pb isotopic systematic of mafic igneous rocks. Geological Magazine 141, 55–62.
Zhang, J.J., Zheng, Y.F., Zhao, Z.F., 2009. Geochemical evidence for interaction between oceanic crust and lithospheric mantle in the origin of Cenozoic continental basalts in east-central China. Lithos 110, 305–326.
Zhao, D., Maruyama, S., Omori, S., 2007. Mantle dynamics of Western Pacific and East Asia: Insight from seismic tomography and mineral physics. Gondwana Research 11, 120–131.
Zhao, G.C., Wilde, S.A., Cawood, P.A., Sun, M., 2001. Archean blocks and their boundaries in the North China Craton: lithological, geochemical, structural and P–T path constraints and tectonic evolution. Precambrian Research 107, 45–73.
Zheng, J.P., Lu, F.X., 1999. Petrologic characteristics of kimberlite-borne mantle xenoliths from the Shandong and Liaoning Peninsula: Paleozoic lithosphere mantle and its heterogeneity. Acta Petrologica Sinica 15, 65–74.
Zhi, X.C., Song, Y., Frey, F.A., Feng, J.L., Zhai, M.Z., 1990. Geochemistry of Hannuoba basalts, eastern China: constraints on the origin of continental alkalic and tholeiitic basalt. Chemical Geology 88, 1–33.
Zhu, R.X., Zheng, T.Y., 2009. Destruction geodynamics of the North China Craton and its Paleoproterozoic plate tectonics. Chinese Science Bulletin 54, 3354–3366.
Zou, H.B., Zindler, A., Xu, X.S., Qi, Q., 2000. Major, trace element, and Nd, Sr and Pb isotope studies of Cenozoic basalts in SE China: mantle sources, regional variations, and tectonic significance. Chemical Geology 171, 33–47.